Amphibian mast cells: barriers to chytrid fungus infections

Authors: Kelsey A. Hauser[1], Christina N. Garvey[1], Ryley S. Crow[1], Muhammad R.H. Hossainey[1], Dustin T. Howard[1], Netra Ranganathan[1], Lindsey K. Gentry[2], Amulya Yaparla[1], Namarta Kalia[1], Mira Zelle[1], Elizabeth J. Jones[3], Anju N. Duttargi[3], Louise A. Rollins-Smith[4,5], Carly R. Muletz-Wolz[2], Leon Grayfer[1]*.

Affiliations:
[1]Department of Biological Sciences, The George Washington University, Washington, DC, USA.

[2]Center for Conservation Genomics, Smithsonian National Zoo & Conservation Biology Institute, Washington, DC, USA.

[3]Department of Oncology, Lombardi Comprehensive Cancer Center, Georgetown University, Washington DC, USA.

[4]Departments of Pathology, Microbiology and Immunology, and of Pediatrics, Vanderbilt University School of Medicine, Nashville, TN, USA.

[5]Department of Biological Sciences, Vanderbilt University, Nashville, TN, USA

*Corresponding author:
Suite 6000, 800 22nd St NW, Washington, DC 20052, USA.
Phone: 202-994-8076
Email: leon_grayfer@gwu.edu.

Keywords: mast cells, chytrid fungus, amphibian immunity, skin immunity

Abstract: Global amphibian declines are compounded by deadly disease outbreaks caused by the chytrid fungus, *Batrachochytrium dendrobatidis* (*Bd*). Much has been learned about the roles of amphibian skin-produced antimicrobial components and microbiomes in controlling *Bd*, yet almost nothing is known about the roles of skin-resident immune cells in anti-*Bd* defenses. Mammalian mast cells reside within and serve as key immune sentinels in barrier tissues like skin. Accordingly, we investigated the roles of *Xenopus laevis* frog mast cells during *Bd* infections. Our findings indicate that enrichment of *X. laevis* skin mast cells confers significant anti-*Bd* protection and ameliorates the inflammation-associated skin damage caused by *Bd* infection. This includes a significant reduction in *Bd*-infected skin infiltration by neutrophils. Augmenting frog skin mast cells promotes greater mucin content within cutaneous mucus glands and protects frogs from *Bd*-mediated changes to their skin microbiomes. Mammalian mast cells are known for their production of the pleiotropic interleukin-4 (IL4) cytokine and our findings suggest that the frog IL4 plays a key role in conferring the effects seen following frog skin mast cell enrichment. Together, this work underlines the importance of amphibian skin-resident immune cells in anti-*Bd* defenses and illuminates a novel avenue for investigating amphibian host-chytrid pathogen interactions.

INTRODUCTION

Catastrophic declines of hundreds of amphibian species across six continents have been causally linked to the chytrid fungi, *Batrachochytrium dendrobatidis* (*Bd*) and *Batrachochytrium salamandrivorans* (*Bsal*)[1, 2]. Motile *Bd* zoospores readily colonize keratinized skin of adult amphibians and keratinized mouthparts of tadpoles[3]. *Bd* skin infections culminate in chytridiomycosis, ultimately disrupting the function of this respiratory and barrier tissue[3, 4, 5]. Effectively combatting chytrid infections requires a holistic understanding of amphibian cutaneous immune defenses. Research efforts up to this point have focused on antifungal capacities of amphibian skin-produced antimicrobial peptides[6, 7]; commensal antifungal products[7, 8, 9]; antifungal properties of mucus[9], alkaloids[10], and lysozymes[11, 12] as well as the roles of antibodies[4, 13]. Many of these studies suggest that *Bd* exposure can elicit some immune protection[14]. However, the contribution of skin-resident immune cells to amphibian anti-*Bd* defenses remains almost entirely unexplored.

Mammalian mast cells serve as sentinels of mucosal and connective tissues, including in barrier tissues like skin, where they maintain homeostasis and regulate immune responses[15]. Other granulocyte-lineage cells such as neutrophils are generally not found in healthy tissues and only extravasate into sites of inflammation[16]. Consequently, mast cells are among the first immune cells to recognize and respond to skin-infiltrating pathogens. When activated, mast cells release pre-formed and *de novo*-generated immunomodulatory compounds that may serve to elicit, exacerbate, or ameliorate inflammatory responses[15]. One of these mast cell-produced mediators, the interleukin-4 (IL4) cytokine dampens inflammation and promotes tissue repair[17]. Cells bearing hallmark mast cell cytology have been reported across a range of non-mammalian species[18, 19], including amphibians[20]. Notably, the principal mast cell growth factor, stem cell factor (SCF, KIT ligand) required for mast cell differentiation and survival[21] is expressed by all vertebrates examined to-date.

Here, we combine comprehensive *in vitro* and *in vivo* approaches to define the roles of amphibian (*Xenopus laevis*) mast cells during *Bd* infections. Our results provide compelling evidence that skin-resident immune cells contribute to anti-*Bd* defenses.

RESULTS

Frog mast cells possess archetypal mast cell cytology and transcriptional profiles

We produced *X. laevis* recombinant (r)SCF, and used this reagent to generate mast cell cultures from bone marrow-derived myeloid precursors[22]. Mast cells were compared to bone marrow-derived neutrophilic granulocytes (hereafter referred to as 'neutrophils'), differentiated using a recombinant *X. laevis* colony-stimulating factor-3[22] (rCSF3, *i.e.*, granulocyte colony-stimulating factor; GCSF). While the neutrophil cultures were comprised of cells with hyper-segmented nuclei and neutral-staining cytoplasms (Fig. 1A), the mast cell cultures consisted predominantly of mononuclear cells with basophilic cytoplasm (Fig. 1B). We confirmed the granulocyte-lineage of *X. laevis* mast cells using specific esterase (SE) staining (Fig. 1D). As expected, *X. laevis* neutrophils were also SE-positive (Fig. 1C). Mast cell and neutrophil morphology was further explored with electron microscopy (Fig. 1E-H). SEM imaging demonstrated that *X. laevis* mast cells possess extensive folding of their plasma membranes (Fig. 1F). This mast cell-characteristic membrane ruffling appeared as projections resembling pseudopods via TEM, which further revealed electron-dense heterogenous granules, few mitochondria, and round to elongated nuclei (Fig. 1H) typical of mammalian mast cells[23]. *X. laevis* neutrophils also exhibited pronounced membrane ruffling (Fig. 1E) but strikingly distinct intracellular appearance including multilobed nuclei (Fig. 1G).

Frog mast cells and neutrophils exhibited distinct transcriptional profiles of immune-related genes including those encoding lineage-specific transcription factors, immune receptors, downstream signaling components and adhesion molecules, as well as non-immune genes (Fig. 1I). Frog mast cells and neutrophils each expressed greater levels of lineage-specific transcription factors associated with mammalian mast cell (gata1, gata2, and mitf)[24] and neutrophil (cebp family members)[25] counterparts, respectively (Fig. 2A). Notably, mast cells expressed greater levels of enzyme and cytokine genes associated with tissue remodeling (carboxypeptidase-3; cpa3[26]), immune suppression (indoleamine 2,3 dioxygenase-1; ido1[27]) and amelioration of cutaneous inflammation (leukemia inhibitory factor, lif[28]; Fig. 2B). Conversely, neutrophils expressed predominantly proinflammatory enzymes and cytokine genes such as leukotriene 4 hydrolase (lta4h; Fig. 2B) and tumor necrosis factor alpha (tnfa, Fig. 2B). In addition, mast cells and neutrophils each had greater expression of genes encoding their respective growth factor receptors, kit and csf3r (Fig. 2B).

Enriching mast cells in frog skin offers protection against *Bd*

Although all granulocyte-lineage cells possess SE activity, mast cells are the predominant mononuclear granulocytes to reside in vertebrate tissues[29]. Therefore, we selectively enriched mast cells in *X. laevis* skin via subcutaneous rSCF administration (note SE-stained cells indicated by arrows in r-ctrl-injected skins, Fig. 3A, versus r-SCF-injected skins, Fig 3B). We confirmed SE-positive cells in rSCF-treated skins also possessed round-oval nuclei (Fig. 3C). Maximum mast cell enrichment was observed 12 hours post injection (hpi) of rSCF (Fig. 3D).

We next examined the consequences of enriching frog skin mast cells on *Batrachochytrium dendrobatidis* (*Bd*) infection outcomes. To this end, *X. laevis* were subcutaneously administered with rSCF or the r-ctrl, infected with *Bd,* and the skin fungal loads assessed at 10- and 21-days post infection (dpi). At 10 dpi, skin mast cell-enriched *X. laevis* possessed significantly lower *Bd* loads than r-ctrl administered animals (Fig. 3E). By 21 dpi, both r-ctrl and rSCF-administered groups possessed substantially greater *Bd* loads, although the mast cell-enriched animals continued to show significantly lower skin fungal loads (Fig. 3E).

Mammalian mast cells may be labeled *in situ* by using avidin to visualize the heparin-containing mast cell granules[30]. Using this approach, we confirmed that frog bone marrow-derived mast cells likewise possess heparin-containing granules (Fig. 4A&B). We next used this staining approach to visualize and enumerate mast cells in the skins of control, mast cell-enriched and *Bd*-challenged animals (Fig. 4C-I). We observed that frog skin mast cell enrichment progressively waned with time in mock-infected animals, and by 21 days post mock infection these animals had skin mast cell numbers comparable to r-ctrl-injected, mock-infected control animals (Fig. 4C, D). Conversely, compared to mock-infected control animals, the rSCF-injected, *Bd*-challenged frogs maintained significantly greater mast cell numbers in their skin throughout the 21-day infection study (Fig. 4C, E-H). Interestingly, r-ctrl-injected, *Bd*-infected animals exhibited significantly increased skin mast cell numbers at 10- and 21-days of infection, compared to uninfected control frogs (Fig. 4C, I). Most of these mast cells were observed in the epidermal layer, spreading out between the skin epithelial cells (Fig. 4G).

Mast cells protect frogs from *Bd*-elicited inflammation-associated pathology

To explore potential mechanisms of mast cell-mediated protection against *Bd,* we compared the gene expression profiles of r-ctrl- and rSCF-administered, *Bd*-infected frog skins at 21 dpi. Among

the top differentially expressed genes, we noted mast cell-enriched, *Bd*-infected skins possessed greater transcripts for genes associated with cutaneous strength and integrity (lamc2)[31], suppression of cell migration (b3gnt3.1)[32], as well as ion and nutrient flow (gjb3l)[33] (Fig. 5A). Moreover, mast cell-enriched *Bd*-challenged skin exhibited greater expression of genes associated with protection of the mucosa and epithelial healing (ttf3.6s)[34] and mucus production (duoxa1.s[35], gabrp[36]; Fig. 5A). In striking contrast, skins from control *Bd*-infected frogs revealed greater expression of genes associated with leukocyte infiltration and inflammation (*e.g.*, ccl19, cxcl16, adamts13, csf3r; Fig. 5A). These transcriptional profiles were supported by our histological observations wherein control *Bd*-infected skins exhibited hyperkeratosis, epidermal hyperplasia, jagged stratum corneum, and extensive leukocyte infiltration (Fig. 5B), while mast cell-enriched *Bd*-infected tissues appeared considerably less afflicted by these pathologies (Fig. 5C). Quantification of *Bd*-infected skin epidermal thickness confirmed that mast cell-enriched animals possessed significantly less thickened epidermal skin compared to control (r-ctrl), *Bd*-infected animals (Fig. 5D).

Because mast cell-enriched frog skins had greater expression of genes associated with mucosal tissue integrity and mucus production (Fig. 5A), we also investigated whether the anti-*Bd* protection identified in mast cell-enriched skins could be due, at least in part, to differences in mucus production. Interestingly, the skin mucus glands of mast cell-enriched, mock- and *Bd*-infected frogs were significantly more filled than those of mock- and *Bd*-infected control animals (Fig. 5B,C,E).

Cutaneous neutrophil enrichment results in increased *Bd* fungal loads

Neutrophils are one of the first leukocytes to infiltrate infected tissues, typically amplifying inflammation[37]. All vertebrate neutrophils depend on CSF3 for their differentiation and function[38], and our previous work has demonstrated the gene encoding the CSF3 receptor (csf3r) is a marker of *X. laevis* neutrophils[39, 40]. Because csf3r expression was markedly elevated in control over mast cell-enriched skins of infected frogs (Fig. 5A), we examined the neutrophil content in the skins of these animals over the 21-day course of *Bd* infection (Fig. 6A-E). To this end, we used *in situ* hybridization analysis of skin-myeloperoxidase, a marker of neutrophils[41]. While the skins of r-ctrl- and rSCF-administered, mock-infected frogs contained relatively few neutrophils (Fig. 6A, E), the skins of r-ctrl-injected, *Bd*-infected animals had significantly elevated neutrophil numbers

(Fig. 6B,C,E). Conversely, at both examined timepoints (10, 21 dpi), mast cell-enriched frog skins possessed neutrophil levels similar to those seen in the uninfected animals (Fig. 6D,E).

We next assessed the consequence of enriching frog skins for neutrophils via subcutaneous rCSF3 administration. We confirmed neutrophil enrichment peaked 12 hp rCSF3 injection (Fig. S1) and resulted in a thickened epidermis in comparison with r-ctrl injected skins of otherwise healthy animals (*i.e.*, no *Bd*; Fig. 6F, G). When challenged with *Bd*, frogs with neutrophil-enriched skin possessed significantly greater *Bd* loads than control frogs (Fig. 6H). This suggests that neutrophil-mediated inflammation may be exacerbating *Bd* infections.

Enrichment of frog skin mast cells alters skin microbial composition

Amphibian skin-produced mucus may offer antimicrobial protection and serve as a selective substratum for commensal microbes, many of which are antifungal[9]. We found no significant differences in direct *Bd*-killing capacities of mucus isolated from mock- or *Bd*-challenged control or mast cell-enriched frogs (Fig. S2). By contrast, we observed substantial differences in skin microbiomes, including changes in bacterial composition and richness as well as relative abundances of *Bd*-inhibitory bacteria (Fig. 7, Fig. S3). A total of 1645 bacterial amplicon sequence variants (ASVs) were identified from 20 bacterial phyla, seven of which were predominant (Fig. 7A). Of these, *Verrucomicrobiota* were only present on uninfected animals, whereas *Acidobacteriota* was only seen after 21 dpi on both control and mast cell-enriched, infected animals (Fig. 7A).

At 10 dpi, mast cell-enrichment resulted in a nominal shift in community composition compared to control frogs (Fig. 7B). Notably, while control, *Bd*-infected animals exhibited a drastic shift in community composition, mast cell-enriched animals possessed substantially less deviated community composition (Fig. 7B), suggesting that these cells are somehow counteracting the adverse effects of *Bd* on microbiome structure. These mast cell-mediated effects persisted to 21 dpi (Fig. S3A).

At 10 dpi, mast cell-enriched and mock-infected frogs possessed significantly greater abundance of *Bd*-inhibitory bacteria such as *Chyrseobacterium sp*., compared to control, mock infected animals (Fig. 7C)[42]. This suggests that mast cells may promote skin flora composition that is more antifungal. Control (non-enriched) *Bd*-infected frogs possessed significantly greater abundance of *Bd*-inhibitory bacteria than all other treatment groups (Fig. 7C). While mast cell-

enriched, *Bd*-infected frogs had lower abundance of *Bd*-inhibitory bacteria than control infected frogs, they possessed higher abundance of inhibitory taxa than uninfected control animals (Fig. 7C). The *Bd*-inhibitory bacteria seen in greater abundance on mast cell-enriched, *Bd*-infected animals, included *Roseateles sp*., *Flavobacterium sp.*, and *Kaistia sp*. We did not see significant differences in *Bd*-inhibitory bacteria across the treatment groups at 21 dpi (Fig. S3B).

Mast cell-enriched uninfected frogs exhibited increased frog skin bacterial richness at 10 dpi (Fig. 7D). While control *Bd*-infected animals exhibited significantly reduced skin microbial richness, mast cell-enriched *Bd*-infected frogs did not exhibit such a reduction in bacterial richness (Fig. 7D), supporting the idea that mast cells may be counteracting the adverse effects of *Bd* on skin microbiome composition.

Frog mast cells alter skin antimicrobial peptide gene expression

Amphibians rely heavily on skin-produced antimicrobial peptides (AMPs) for antifungal protection[43], and mast cells produce antimicrobial AMPs[44]. We thus examined whether mast cells could be sources of such AMPs during *Bd* infections. As anticipated, *Bd*-challenged mast cells, but not *Bd*-challenged neutrophils upregulated their expression of the AMP-encoding genes, *pgla* and magainin (*mag*, Fig. 8A).

To follow up these observations *in vivo*, we examined *pgla* and *mag* gene expression in the skins of mast cell-enriched and *Bd*-challenged animals. Compared to control (r-ctrl) animals, mast cell-enriched frogs did not have elevated mRNA levels of *mag* or *pgla* after 12 hrs of rSCF administration (Fig. S4A&B). After 10 days of mock-infection, mast cell-enriched animals possessed significantly greater skin expression of *mag* and *pgla* than control animals (Fig. S4A&B). We did not see significant differences in skin *mag* or *pgla* gene expression between *Bd*-challenged control and mast cell-enriched frogs after 10 dpi (Fig. S4). By 21 days of challenge, the rSCF-administered mock-infected frogs possessed lower gene expression levels of both AMPs (significantly so for *pgla*, Fig. S4A&B), possibly due to some sort of compensatory effect. At 21 dpi, mast cell-enriched frog skins had greater (albeit not significantly so) *pgla* expression than control frogs (Fig. S4B).

Frog mast cell-expressed interleukin-4 confers anti-*Bd* protection

Mammalian mast cells are recognized as potent producers of the pleotropic anti-inflammatory cytokine, interleukin-4 (*il4*)[45]. Notably, *X. laevis* mast cells challenged *in vitro* with *Bd* significantly upregulated their *il4* gene expression, whereas almost no *il4* expression was detected from either unstimulated or *Bd*-challenged neutrophils (Fig. 8A).

When we examined the expression of *il4* in the skin of control and mast cell-enriched animals, we found that 12 hours following rSCF administration (time of *Bd* challenge), the mast cell enriched frog skins possessed significantly greater transcripts of *il4* than control animals (Fig. 8B). By 10 and 21 dpi, both control and mast cell-enriched mock-infected animals possessed baseline skin il4 expression (Fig. 8B). At 10 days of *Bd* infection, control animals possessed increased (not significantly) skin *il4* gene expression whereas mast cell-enriched frog skins had significantly elevated *il4* transcript levels (Fig. 8B). By 21 dpi, *Bd*-infected control animals had baseline skin *il4* expression and the mast cell enriched animals had elevated, albeit not significant expression of this cytokine gene in their skins (Fig. 8B).

To examine whether IL4 could confer the anti-*Bd* effects seen following frog skin mast cell enrichment, we produced this *X. laevis* cytokine in recombinant form (rIL4) and confirmed that subcutaneous injection of rIL4 augmented expression of genes typically activated by the mammalian IL4[46] (cd36, metalloproteinase inhibitor 3-timp3, and monoamine oxidase A-maoa; Fig. S5A).

We next administered frogs subcutaneously with rIL4 or r-ctrl, challenged them with *Bd* and examined the key parameters affected by skin mast cell-enrichment, including skin mucus gland filling, skin *Bd* loads, and reduction in *Bd*-associated skin inflammation. When we examined the mucus content of control and rIL4-administered animals, we found that frogs treated with rIL4 possessed greater skin mucus gland filling than control animals and irrespective of mock- or *Bd*-challenge (Fig. 8C-E). At 21 dpi (but not at 10 dpi), rIL4-administered frogs possessed significantly lower skin *Bd* loads (Fig. 8F) and exhibited significantly less epidermal thickening (Fig. 8C,D,G) and less neutrophil infiltration (Fig. 8H-J) than control animals. Conversely, subcutaneous administration of rIL4 to animals with active *Bd*-infection did not alter their fungal loads (Fig. S5B), suggesting a critical point during which IL4 may offer protection against this fungal pathogen.

DISCUSSION

Amphibian extinction rates far outpace those of any other vertebrate class[47]. It is now well-established that chytrid fungi are major contributors to these declines, and strikingly, are considered the greatest infectious disease threat to biodivsersity[48]. The development of effective mitigation strategies though, is hindered by incomplete understanding of amphibian immune defenses and skin integrity. In this respect, while mast cells are recognized as key immune sentinels of tissues such as skin[49], relatively little is known about this cell lineage outside of mammals. Our findings provide the first in-depth functional analyses of these cells in amphibians and explore their protective mechanisms during chytrid infections. This work presents a unique perspective on the evolution of mast cell functionality and will serve as a new avenue to explore ways to counteract the amphibian declines.

Mammalian mast cells are potent producers of the pleotropic anti-inflammatory interleukin-4 (IL4)[45] cytokine and our findings suggest that this is also true of frog mast cells. In mammals, IL4 also plays roles in tissue repair[17] and mucus production by intestinal goblet cells[50], which aids in the 'weep and sweep' pathogen elimination and may contribute to the maintenance of commensal communities in the gut[51]. This is consistent with our findings, which suggest that IL4 may be a central means by which frog mast cells confer protection against *Bd,* by counteracting *Bd*-elicited inflammation, including minimizing neutrophil infiltration, maintaining skin integrity, and promoting mucus production by skin mucus glands. The outcomes of cytokine signaling are critically dependent on timing, locations, and context[50]. This possibly explains why administering rIL4 prior to *Bd* challenge results in significant anti-*Bd* protection whereas treating already infected animals with this cytokine did not reduce fungal loads.

We anticipate that in addition to IL4 production, frog mast cells confer the observed antifungal protection through a myriad of additional mechanisms. Indeed, we observed elevated expression of antimicrobial peptide genes in the skins of mock-infected mast cell-enriched frogs 10 days after rSCF administration. The fact that we did not see the same expression patterns following *Bd* challenge could potentially reflect the highly immunomodulatory capacities of this pathogen[52]. Undoubtedly, frog skin-resident mast cells have evolved to contribute to and modulate skin antifungal antimicrobial peptide production just as *Bd* has undoubtedly coevolved to target this aspect of amphibian skin defenses.

Bd infections caused major reductions in bacterial taxa richness, changes in composition and substantial increases in the relative abundance of *Bd*-inhibitory bacteria early in the infection. Similar changes to microbiome structure occur during experimental *Bd* infections, such as in red-backed salamanders and mountain yellow-legged frogs[8, 53]. In turn, progressing *Bd* infections corresponded with a return to baseline levels of *Bd*-inhibitory bacteria abundance and rebounding microbial richness, albeit with dissimilar communities to those seen in control animals. These temporal changes indicate that amphibian microbiomes are dynamic, as are the effects of *Bd* infections on them. Indeed, *Bd* infections may have long-lasting impacts on amphibian microbiomes[8], including the possible establishment of 'ecological memory', resulting in greater adaptation to subsequent pathogen exposures[9, 54]. While *Bd* infections manifested in these considerable changes to frog skin microbiome structure, mast cell enrichment appeared to counteract the deleterious effects to their microbial composition. It will thus be interesting to learn from future studies how frog mast cells impact skin microbiome ecological memory. Presumably, the greater skin mucosal integrity and mucus production observed after mast cell enrichment served to stabilize the cutaneous environment during *Bd* infections, thereby ameliorating the *Bd*-mediated microbiome changes. While this work explored the changes in established antifungal flora, we anticipate the mast cell-mediated inhibition of *Bd* may be due to additional, yet unidentified bacterial, viral, or fungal taxa. Intriguingly, while mammalian skin mast cell functionality depends on microbiome elicited SCF production by keratinocytes[55], our results indicate that frog skin mast cells in turn impact skin microbiome structure and likely their function. It will be interesting to further explore the interdependent nature of amphibian skin microbiomes and resident mast cells.

In contrast to the mast cell-mediated effects, enrichment of neutrophils seemed to result in greater *Bd* skin burdens. This suggests that neutrophils may result in a greater level of inflammation, which is not protective in the context of *Bd* infections. This is consistent with other studies that suggest that a strong immune response in the skin compartment of some species may be detrimental[56, 57].

Amphibian skin is much thinner and more permeable than that of mammals[7], and as such, arguably represents a more penetrable barrier to pathogens. Because mammalian skin is relatively impermeable, mast cells are absent from healthy mammalian epidermises and are instead found exclusively in their dermal layers[58]. However, mammalian mast cells may infiltrate the skin

epidermal layer during diseases such as dermatitis[59]. In contrast, we showed here and have observed across several classes of amphibians[16] that mast cells are found in both epidermal and dermal layers. This localization has presumably evolved to support the more intimate contact between amphibian skin and their environments. Considering the importance of amphibian cutaneous integrity to their physiology[60], it is likely that skin-resident mast cells co-evolved to support skin immunity, physiology, and symbiotic microbiota. Ongoing research continues to reveal functional differences between mammalian connective tissue and mucosa-resident mast cells[61], and we suspect that there is similarly much to learn about the distinct physiological and immune roles of amphibian epidermal and dermal mast cells.

Mammalian mast cells are thought to arise from two distinct lineages. Fetal-derived progenitors seed peripheral tissues during the neonatal life[62] and mature into long-lived connective tissue mast cells (CTMCs)[63]. Conversely, inducible mucosal mast cells (MMCs) arise from bone marrow–derived mast cell progenitors (MCps) and are recruited to mucosal tissues in response to inflammation[64, 65]. The connective tissue mast cells are thought to possess significantly greater levels of heparin than bone marrow-derived mast cells[66]. Interestingly, the *in vitro* frog bone marrow-derived mast cells possessed substantially lower heparin content than what we observed in the skin-resident and *Bd*-recruited mast cells. Unlike the mammalian skin, frog skin is both a connective tissue and a mucosal barrier, begging the question of how the frog skin mast cells compare to the mammalian CTMCs and MMCs. It is interesting to consider that frog skin mast cells observed at steady state, following rSCF-enrichment, and recruited/expanded in response to *Bd*, all had substantial heparin levels. Possibly, the expansion of frog skin mast cell numbers in response to both rSCF and *Bd* is facilitated by skin-resident precursors, explaining the high heparin content observed in these populations. Of course, it is equally possible that amphibian mast cell ontogeny and heparin content are not the same as mammals. It will be invaluable to learn with future studies the origins, fates and immune consequences of distinct frog skin mast cell lineages and subsets.

It has become apparent that amphibian host-*Bd* interactions are highly complex and multifaceted while different amphibian species exhibit marked differences in their susceptibilities to this devastating pathogen[2, 4]. The findings described here emphasize the importance of skin-resident mast cells for successful anti-*Bd* defenses and demonstrate that these immune sentinels are intimately linked to many aspects of frog skin physiology. Our results indicate that when mast

cells are enriched, the ensuing changes in the skin allow for greater resistance to infection by developing zoospores. Presumably, distinct amphibian species have evolved disparate interconnections between their skin mast cells and their cutaneous defenses, as dictated by their respective physiological and environmental pressures. In turn, these species-specific differences likely dictate whether and to what extent the skin-resident mast cells of a given amphibian species recognize and appropriately respond to *Bd* infections. We postulate that such differences may contribute to the differences in susceptibilities of amphibian species to pathogens like chytrid fungi. Greater understanding of these relationships across disparate amphibian species holds promise of harnessing this knowledge towards possible development of preventative and therapeutic strategies against infectious diseases like chytridiomycosis.

METHODS

Animals

Outbred 1 year-old (1.5-2”), mixed sex *X. laevis* were purchased from Xenopus 1 (Dexter, MI). All animals were housed and handled under strict laboratory regulations as per GWU IACUC (Approval number 15-024).

Recombinant cytokines and bone marrow granulocyte cultures

The *X. laevis* rSCF, rCSF3 and rIL4 were generated as previously described for rCSF3[67] and as detailed in the supplemental materials.

Bone marrow isolation, culture conditions, and establishment of neutrophil cultures have been previously described[68]. Mast cell cultures were generated according to protocols adapted from Koubourli et al. (2018) and Meurer et al. (2016) [69, 70]. Isolated bone marrow cells were treated with 250 ng/µl of rSCF on Day 0, Day 4, Day 7, and collected for further analysis on Day 9. Cell cultures were maintained at 27°C with 5% CO_2 in amphibian medium supplemented with 10% fetal bovine serum and 0.25% *X. laevis* serum. Neutrophil-like granulocytes were generated as above but with 250 ng/µl of rCSF3 on Day 0, Day 3, and collected for further analysis on Day 5. Cell cultures were maintained at 27°C with 5% CO_2 in amphibian serum-free medium supplemented with 10% fetal bovine serum, 0.25% *X. laevis* serum, 10 µg/mL gentamicin (Thermo Fisher Scientific, Waltham, Massachusetts, USA), 100 U/mL penicillin, and 100 µg/mL streptomycin (Gibco, Thermo Fisher Scientific).

Enrichment of skin granulocyte subsets

Animals were subcutaneously injected between the skin and muscle layers with 5 µg/animal of rSCF, rCSF3, or r-ctrl in 5 µL of saline using finely pulled glass needles. Optimal time course and dose for *in vivo* mast cell and neutrophil enrichment were determined during preliminary experiments.

Recombinant interleukin-4 treatment

The capacity of the recombinant interleukin-4 (rIL4) to induce expression of genes associated with mammalian IL4 responses were assessed by injecting frogs (*N*=6 per treatment group subcutaneously with rIL4 (5 µg/animal) or r-ctrl in 5 µl of saline. After 6hrs, animals were sacrificed, and skins were isolated for gene expression analyses.

To examine the effect of rIL4 on *Bd* loads, frogs were infected with *Bd* by water bath (10^5 zoospores/mL) as described below and 1 day later injected subcutaneously, dorsally with rIL4 (5 µg/animal) or r-ctrl in 5 µl of saline. After an additional 9 days of infection, animals were sacrificed and their dorsal skin *Bd* loads examined.

***Bd* stocks and fungal challenge**

Bd isolate JEL 197 was grown in 1% tryptone broth or on 1% tryptone agar plates (Difco Laboratories, Detroit, MI) supplemented with 100 U/mL penicillin and 100 µg/mL streptomycin (Gibco) at 19°C.

In vitro Bd killing was evaluated by incubating live *Bd* (maturing zoosporangia) with mast cells or neutrophils at ratios of 5:1 or 1:1 *Bd* cells per granulocyte. Cells were incubated at 27°C for three days before fungal loads were analyzed by absolute qPCR. Experimental groups were compared to pathogen DNA amounts derived from equal quantities of live *Bd* plated alone in otherwise identical conditions.

For *in vivo* infection studies, zoospores were harvested by flooding confluent tryptone agar plates with 2 mL sterile A-PBS for 10 minutes. Twelve hours post rSCF, rCSF3, rIL4, or r-ctrl injection, animals were infected with 10^7 zoospores or mock-infected in 100 mL of water (10^5 zoospores/mL). After 3 hrs, 400 mL of water was added to each tank. Skins were collected for

histology and gene expression analyses on 1, 10, and 21 dpi with 10 and 21 dpi representing intermediate and later timepoints of infection, respectively.

Histology

Leukocyte cytology and cutaneous SE staining has been described[67] and is detailed in the supplemental materials. An Alcian Blue/PAS staining kit (Newcomer Supply, Middleton, WI) was used to quantify mucin content. Histology is detailed in the supplemental materials.

Electron Microscopy

Processing and imaging of cells for transmission and scanning electron microscopy (TEM and SEM) was conducted at the GWU Nanofabrication and Imaging Center (GWNIC). For transmission electron microscopy, cells were fixed as monolayers on six-well plates with 2.5% glutaraldehyde and 1% paraformaldehyde in 0.1 M sodium cacodylate buffer for one hour. Cells were treated with 1% osmium tetroxide in 0.1 M sodium cacodylate buffer for 1 hr. Following washes, cells were *en bloc* stained with 1% uranyl acetate in water overnight at 4°C. Samples were dehydrated through an ethanol series and embedded in epoxy resin using LX112. Inverted Beem capsules were placed into each tissue culture well to create *on face* blockfaces for sectioning. Resin was cured for 48 hrs at 60°C. The 95 nm sections were post-stained with 1% aqueous uranyl acetate and Reynold's lead citrate. All imaging was performed at 80 KV in a Talos 200X transmission electron microscope (Thermo Fisher Scientific, Hillsboro, OR).

For SEM, cells were fixed with 2.5% glutaraldehyde / 1% paraformaldehyde in Sodium cacodylate buffer, followed by 1% OsO_4, then dehydrated through an ethyl alcohol series. Coverslips were critical point dried and coated with 2 nm iridium. Cells were imaged using a Teneo Scanning Electron Microscope (Thermo Fisher Scientific).

Analyses of immune gene expression and *Bd* skin loads

These analyses have been described[67] and are detailed in supplemental materials.

RNA sequencing

For transcriptomic profiling, bone marrow-derived neutrophil and mast cell cultures were generated as described above and FACS-sorted according to preestablished size and internal

complexity parameters to isolate the respective subsets for further analyses. Sorted cells were immediately processed to extract and purify RNA. Flash frozen samples were sent to Azenta Life Sciences for all library preparation, RNA sequencing, and analyses. In short, polyadenylated RNA was isolated using Oligo dT beads. Enriched mRNAs were then fragmented for first and second strand cDNA synthesis. cDNA fragments were end repaired, 5' phosphorylated, and dA-tailed. Fragments were then ligated to universal adaptors and PCR-amplified. 150-bp paired-end sequencing was performed on an Illumina HiSeq platform.

FastQC was used to evaluate raw data quality. Adaptors sequences and poor-quality nucleotides were removed from reads using Trimmomatic v.0.36. The STAR aligner v.2.55.2b was used to map these reads to the Xenopus_laevis_9_2 reference genome from ENSEMBL. To determine differential gene expression, featureCount (Subread package v.1.5.2) was first used to count unique gene hits, which were then used with DESeq2 to calculate absolute $\log_2$-fold change.

Skin microbiome analyses

Towards microbiome studies, frogs were housed individually (N=6/treatment group). At indicated times, frogs were gently rinsed with sterile deionized water to remove transient microbes and gently swabbed 20 times, dorsally. Genomic DNA was extracted from swabs using a PowerSoil Pro kit on a Qiacube HT (QIAGEN, MD). One-step PCR library prep and dual-index paired-end Illumina sequencing was used to sequence the skin microbiome of individual frogs. A ~380 base pair region in the V3-V5 region of the 16S rRNA gene using the universal primers 515F-Y (GTGYCAGCMGCCGCGGTAA) and 939R (CTTGTGCGGGCCCCCGTCAATTC) was used for amplification. Negative and positive controls (ZymoBIOMICS D6300 & D6305, Zymo, CA) were included in each round of extraction and PCR. Reactions were done in duplicate for each sample, pooled, cleaned with in-house Speed-beads (in a PEG/NaCl buffer), quantified with a Qubit4 (Invitrogen, MA) and pooled into a final library in equimolar proportion. The pooled library was sequenced on two Illumina MiSeq runs (v3 chemistry: 2x300 bp kit) at the Center for Conservation Genomics, Smithsonian National Zoo & Conservation Biology Institute.

Analyses were performed in the R environment version 4.0.3 (R Core Team, 2020) using methods detailed in the supplemental materials.

Statistical analyses

Differences in transcript expression were calculated with one-way or multi-way ANOVAs followed by Tukey post-hoc tests. Student's t-tests were used to determine differences in *Bd* loads between treatments only. Statistical differences in mucin content and mucosome *Bd*-killing were assessed with the two-way ANOVA calculator available online through Statistics Kingdom. For RNA sequencing, *p*-values were calculated with the Wald test and were adjusted using the Benjamini-Hochberge procedure.

ACKNOWLEDGMENTS:

We thank Dr. Cynthia S. Dowd and Ben England (Chemistry Department, GWU) for their help with *X. laevis* mucus lyophilization. We thank Dr. Christine Brantner (GWU Nanofabrication and imaging center) for assistance with TEM and SEM imaging. KAH, MRHH, and AY were supported by Wilbur V. Harlan summer graduate research fellowships. We thank Dr. Alexander Jeremic (GWU) for access to and use of his confocal microscope. We thank Dr. Gregory Cresswell (GWU) for his help with flow cytometry and cell sorting. KAH, MRHH, NR, NK, AY, MZ, and LG thank the GWU Biology Department. We thank the three anonymous reviewers whose insightful comments and suggestions helped to improve the scope and breadth of this manuscript.

Funding:

National Science Foundation grant 2131061 (LG, CRMW)
National Science Foundation grant 2147466 (LG)
National Science Foundation grant 2147467 (LAR-S)

Author contributions:

Conceptualization: KAH, LG
Methodology: KAH, CNG, RSC, MRHH, DTH, NR, LKG, AY, NK, MZ, EJJ, AND, LAR-S, CRMW, LG
Investigation: KAH, CNG, RSC, MRHH, DTH, NR, LKG, AY, NK, MZ, EJJ, AND, LAR-S, CRMW, LG
Visualization: KAH, CNG, RSC, EJJ, AND, LG
Funding acquisition: LG, CRMW, LAR-S
Project administration: LG
Supervision: LG, CRMW, LAR-S
Writing – original draft: KAH, LAR-S, CRMW, LG
Writing – review & editing: KAH, LAR-S, CRMW, LG

Competing interests: The authors declare no competing interests.

Data and materials availability: All data are available in the main text or the supplementary materials.

REFERENCES

1. Martel, A. *et al.* Wildlife disease. Recent introduction of a chytrid fungus endangers Western Palearctic salamanders. *Science* 346, 630-631 (2014).
2. Scheele, B.C. *et al.* Amphibian fungal panzootic causes catastrophic and ongoing loss of biodiversity. *Science* 363, 1459-1463 (2019).
3. Van Rooij, P., Martel, A., Haesebrouck, F. & Pasmans, F. Amphibian chytridiomycosis: a review with focus on fungus-host interactions. *Veterinary research* 46, 1-22 (2015).
4. Van Rooij, P. *et al.* Development of in vitro models for a better understanding of the early pathogenesis of Batrachochytrium dendrobatidis infections in amphibians. *Altern Lab Anim* 38, 519-528 (2010).
5. Voyles, J. *et al.* Pathogenesis of chytridiomycosis, a cause of catastrophic amphibian declines. *Science* 326, 582-585 (2009).
6. Rollins-Smith, L.A. The importance of antimicrobial peptides (AMPs) in amphibian skin defense. *Dev Comp Immunol* 142, 104657 (2023).
7. Varga, J.F.A., Bui-Marinos, M.P. & Katzenback, B.A. Frog Skin Innate Immune Defences: Sensing and Surviving Pathogens. *Front Immunol* 9, 3128 (2018).
8. Jani, A.J. *et al.* The amphibian microbiome exhibits poor resilience following pathogen-induced disturbance. *ISME J* 15, 1628-1640 (2021).
9. Woodhams, D.C., McCartney, J., Walke, J.B. & Whetstone, R. The adaptive microbiome hypothesis and immune interactions in amphibian mucus. *Dev Comp Immunol*, 104690 (2023).
10. Rodriguez, C., Rollins-Smith, L., Ibanez, R., Durant-Archibold, A.A. & Gutierrez, M. Toxins and pharmacologically active compounds from species of the family Bufonidae (Amphibia, Anura). *J Ethnopharmacol* 198, 235-254 (2017).
11. Grogan, L.F. *et al.* Review of the Amphibian Immune Response to Chytridiomycosis, and Future Directions. *Front Immunol* 9, 2536 (2018).
12. Rollins-Smith, L.A. *et al.* Immune defenses of Xenopus laevis against Batrachochytrium dendrobatidis. *Front Biosci (Schol Ed)* 1, 68-91 (2009).
13. Ramsey, J.P., Reinert, L.K., Harper, L.K., Woodhams, D.C. & Rollins-Smith, L.A. Immune defenses against Batrachochytrium dendrobatidis, a fungus linked to global amphibian declines, in the South African clawed frog, Xenopus laevis. *Infect Immun* 78, 3981-3992 (2010).
14. McMahon, T.A. *et al.* Amphibians acquire resistance to live and dead fungus overcoming fungal immunosuppression. *Nature* 511, 224-227 (2014).
15. Sobiepanek, A. *et al.* The multifaceted roles of mast cells in immune homeostasis, infections and cancers. *International Journal of Molecular Sciences* 23, 2249 (2022).
16. Hauser, K.A., Garvey, C.N., Popovic, M. & Grayfer, L. Biology of amphibian granulocytes - From evolutionary pressures to functional consequences. *Dev Comp Immunol* 140, 104623 (2023).
17. Allen, J.E. IL-4 and IL-13: Regulators and Effectors of Wound Repair. *Annu Rev Immunol* 41, 229-254 (2023).
18. McNeil, H.P., Adachi, R. & Stevens, R.L. Mast cell-restricted tryptases: structure and function in inflammation and pathogen defense. *Journal of Biological Chemistry* 282, 20785-20789 (2007).
19. Abraham, S.N. & St John, A.L. Mast cell-orchestrated immunity to pathogens. *Nature reviews.Immunology* 10, 440-452 (2010).

20. Baccari, G.C., Pinelli, C., Santillo, A., Minucci, S. & Rastogi, R.K. Mast cells in nonmammalian vertebrates: an overview. *International review of cell and molecular biology* 290, 1-53 (2011).
21. Ito, T. *et al.* Stem cell factor programs the mast cell activation phenotype. *J Immunol* 188, 5428-5437 (2012).
22. Yaparla, A., Wendel, E.S. & Grayfer, L. The unique myelopoiesis strategy of the amphibian Xenopus laevis. *Developmental & Comparative Immunology* 63, 136-143 (2016).
23. Espinosa-Riquer, Z.P. *et al.* Signal transduction pathways activated by innate immunity in mast cells: translating sensing of changes into specific responses. *Cells* 9, 2411 (2020).
24. Cildir, G. *et al.* Understanding mast cell heterogeneity at single cell resolution. *Trends in Immunology* 42, 523-535 (2021).
25. Paudel, S., Ghimire, L., Jin, L., Jeansonne, D. & Jeyaseelan, S. Regulation of emergency granulopoiesis during infection. *Front Immunol* 13, 961601 (2022).
26. Atiakshin, D. *et al.* Carboxypeptidase A3-A Key Component of the Protease Phenotype of Mast Cells. *Cells* 11 (2022).
27. Baban, B. *et al.* IDO activates regulatory T cells and blocks their conversion into Th17-like T cells. *J Immunol* 183, 2475-2483 (2009).
28. Banner, L.R., Patterson, P.H., Allchorne, A., Poole, S. & Woolf, C.J. Leukemia inhibitory factor is an anti-inflammatory and analgesic cytokine. *J Neurosci* 18, 5456-5462 (1998).
29. Agis, H. *et al.* Mast Cell-Lineage Versus Basophil Lineage Involvement in Myeloproliferative and Myelodysplastic Syndromes: Diagnostic Role of Cell-Immunopheno typing. *Leukemia & lymphoma* 22, 187-204 (1996).
30. Tharp, M.D., Seelig, L.L., Jr., Tigelaar, R.E. & Bergstresser, P.R. Conjugated avidin binds to mast cell granules. *J Histochem Cytochem* 33, 27-32 (1985).
31. Kiritsi, D., Has, C. & Bruckner-Tuderman, L. Laminin 332 in junctional epidermolysis bullosa. *Cell Adh Migr* 7, 135-141 (2013).
32. Ho, W.L. *et al.* B3GNT3 expression suppresses cell migration and invasion and predicts favorable outcomes in neuroblastoma. *Cancer Sci* 104, 1600-1608 (2013).
33. Chang, E.H., Van Camp, G. & Smith, R.J. The role of connexins in human disease. *Ear Hear* 24, 314-323 (2003).
34. Taupin, D. & Podolsky, D.K. Trefoil factors: initiators of mucosal healing. *Nat Rev Mol Cell Biol* 4, 721-732 (2003).
35. Fischer, H. Mechanisms and function of DUOX in epithelia of the lung. *Antioxid Redox Signal* 11, 2453-2465 (2009).
36. Wang, A. *et al.* Inhibition of Gabrp reduces the differentiation of airway epithelial progenitor cells into goblet cells. *Exp Ther Med* 22, 720 (2021).
37. Wang, J. Neutrophils in tissue injury and repair. *Cell Tissue Res* 371, 531-539 (2018).
38. Roberts, A.W. G-CSF: a key regulator of neutrophil production, but that's not all! *Growth Factors* 23, 33-41 (2005).
39. Koubourli, V.D., Wendel, E.S., Yaparla, A., Ghaul, J.R. & Grayfer, L. Immune roles of amphibian (Xenopus laevis) tadpole granulocytes during Frog Virus 3 ranavirus infections. *Dev Comp Immunol* 72, 112-118 (2017).
40. Yaparla, A., Wendel, E.S. & Grayfer, L. The unique myelopoiesis strategy of the amphibian Xenopus laevis. *Dev Comp Immunol* 63, 136-143 (2016).

41. Buchan, K.D. *et al.* A transgenic zebrafish line for in vivo visualisation of neutrophil myeloperoxidase. *PLoS One* 14, e0215592 (2019).
42. Woodhams, D.C. *et al.* Antifungal isolates database to centralize data on amphibian ski associated bacteria and their function against emerging fungal pathogens including Batrachochytrium dendrobatidis. *Ecology* 96, 595 (2015).
43. Patocka, J., Nepovimova, E., Klimova, B., Wu, Q. & Kuca, K. Antimicrobial peptides: amphibian host defense peptides. *Current medicinal chemistry* 26, 5924-5946 (2019).
44. Di Nardo, A., Yamasaki, K., Dorschner, R.A., Lai, Y. & Gallo, R.L. Mast cell cathelicidin antimicrobial peptide prevents invasive group A Streptococcus infection of the skin. *J Immunol* 180, 7565-7573 (2008).
45. Babina, M., Guhl, S., Artuc, M. & Zuberbier, T. IL-4 and human skin mast cells revisited: reinforcement of a pro-allergic phenotype upon prolonged exposure. *Archives of dermatological research* 308, 665-670 (2016).
46. Bhattacharjee, A. *et al.* IL-4 and IL-13 employ discrete signaling pathways for target gene expression in alternatively activated monocytes/macrophages. *Free Radic Biol Med* 54, 1-16 (2013).
47. https://www.iucnredlist.org/resources/summary-statistics, I.R.L.
48. Fisher, M.C. & Garner, T.W. Chytrid fungi and global amphibian declines. *Nature Reviews Microbiology* 18, 332-343 (2020).
49. St. John, A.L., Rathore, A.P. & Ginhoux, F. New perspectives on the origins and heterogeneity of mast cells. *Nature Reviews Immunology* 23, 55-68 (2023).
50. Redpath, S.A., Heieis, G. & Perona-Wright, G. Spatial regulation of IL-4 signalling in vivo. *Cytokine* 75, 51-56 (2015).
51. Drago, L. *et al.* Bacteria Living in Biofilms in Fluids: Could Chemical Antibiofilm Pretreatment of Culture Represent a Paradigm Shift in Diagnostics? *Microorganisms* 12 (2024).
52. Rollins-Smith, L.A. & Le Sage, E.H. Batrachochytrium fungi: stealth invaders in amphibian skin. *Curr Opin Microbiol* 61, 124-132 (2021).
53. Muletz-Wolz, C.R., Fleischer, R.C. & Lips, K.R. Fungal disease and temperature alter skin microbiome structure in an experimental salamander system. *Mol Ecol* 28, 2917-2931 (2019).
54. Letourneau, J. *et al.* Ecological memory of prior nutrient exposure in the human gut microbiome. *ISME J* 16, 2479-2490 (2022).
55. Wang, Z. *et al.* Skin microbiome promotes mast cell maturation by triggering stem cell factor production in keratinocytes. *J Allergy Clin Immunol* 139, 1205-1216 e1206 (2017).
56. Ellison, A.R. *et al.* More than skin deep: functional genomic basis for resistance to amphibian chytridiomycosis. *Genome Biol Evol* 7, 286-298 (2014).
57. Savage, A.E., Gratwicke, B., Hope, K., Bronikowski, E. & Fleischer, R.C. Sustained immune activation is associated with susceptibility to the amphibian chytrid fungus. *Mol Ecol* 29, 2889-2903 (2020).
58. Cowen, T., Trigg, P. & Eady, R.A. Distribution of mast cells in human dermis: development of a mapping technique. *Br J Dermatol* 100, 635-640 (1979).
59. Imayama, S., Shibata, Y. & Hori, Y. Epidermal mast cells in atopic dermatitis. *Lancet* 346, 1559 (1995).

60. Larsen, E.H. Dual skin functions in amphibian osmoregulation. *Comparative Biochemistry and Physiology Part A: Molecular & Integrative Physiology* 253, 110869 (2021).
61. West, P.W. & Bulfone-Paus, S. Mast cell tissue heterogeneity and specificity of immune cell recruitment. *Front Immunol* 13, 932090 (2022).
62. Gentek, R. *et al.* Hemogenic Endothelial Fate Mapping Reveals Dual Developmental Origin of Mast Cells. *Immunity* 48, 1160-1171 e1165 (2018).
63. Dwyer, D.F., Barrett, N.A., Austen, K.F. & Immunological Genome Project, C. Expression profiling of constitutive mast cells reveals a unique identity within the immune system. *Nat Immunol* 17, 878-887 (2016).
64. Bankova, L.G., Dwyer, D.F., Liu, A.Y., Austen, K.F. & Gurish, M.F. Maturation of mast cell progenitors to mucosal mast cells during allergic pulmonary inflammation in mice. *Mucosal Immunol* 8, 596-606 (2015).
65. Li, Z. *et al.* Adult Connective Tissue-Resident Mast Cells Originate from Late Erythro-Myeloid Progenitors. *Immunity* 49, 640-653 e645 (2018).
66. Herrera-Heredia, S.A. *et al.* Heparin is required for the formation of granules in connective tissue mast cells. *Front Immunol* 13, 1000405 (2022).
67. Hauser, K. *et al.* Discovery of granulocyte-lineage cells in the skin of the amphibian Xenopus laevis. *FACETS* 5, 571 (2020).
68. Yaparla, A. & Grayfer, L. Isolation and culture of amphibian (Xenopus laevis) sub-capsular liver and bone marrow cells. *Xenopus: Methods and Protocols*, 275-281 (2018).
69. Koubourli, D.V., Yaparla, A., Popovic, M. & Grayfer, L. Amphibian (Xenopus laevis) interleukin-8 (CXCL8): a perspective on the evolutionary divergence of granulocyte chemotaxis. *Frontiers in immunology*, 2058 (2018).
70. Meurer, S.K. *et al.* Isolation of mature (peritoneum-derived) mast cells and immature (bone marrow-derived) mast cell precursors from mice. *PLoS One* 11, e0158104 (2016).
71. Callahan, B.J. *et al.* DADA2: High-resolution sample inference from Illumina amplicon data. *Nat Methods* 13, 581-583 (2016).
72. McMurdie, P.J. & Holmes, S. phyloseq: an R package for reproducible interactive analysis and graphics of microbiome census data. *PLoS One* 8, e61217 (2013).
73. Davis, N.M., Proctor, D.M., Holmes, S.P., Relman, D.A. & Callahan, B.J. Simple statistical identification and removal of contaminant sequences in marker-gene and metagenomics data. *Microbiome* 6, 226 (2018).
74. Jimenez, R.R. *et al.* Inhibitory Bacterial Diversity and Mucosome Function Differentiate Susceptibility of Appalachian Salamanders to Chytrid Fungal Infection. *Appl Environ Microbiol* 88, e0181821 (2022).

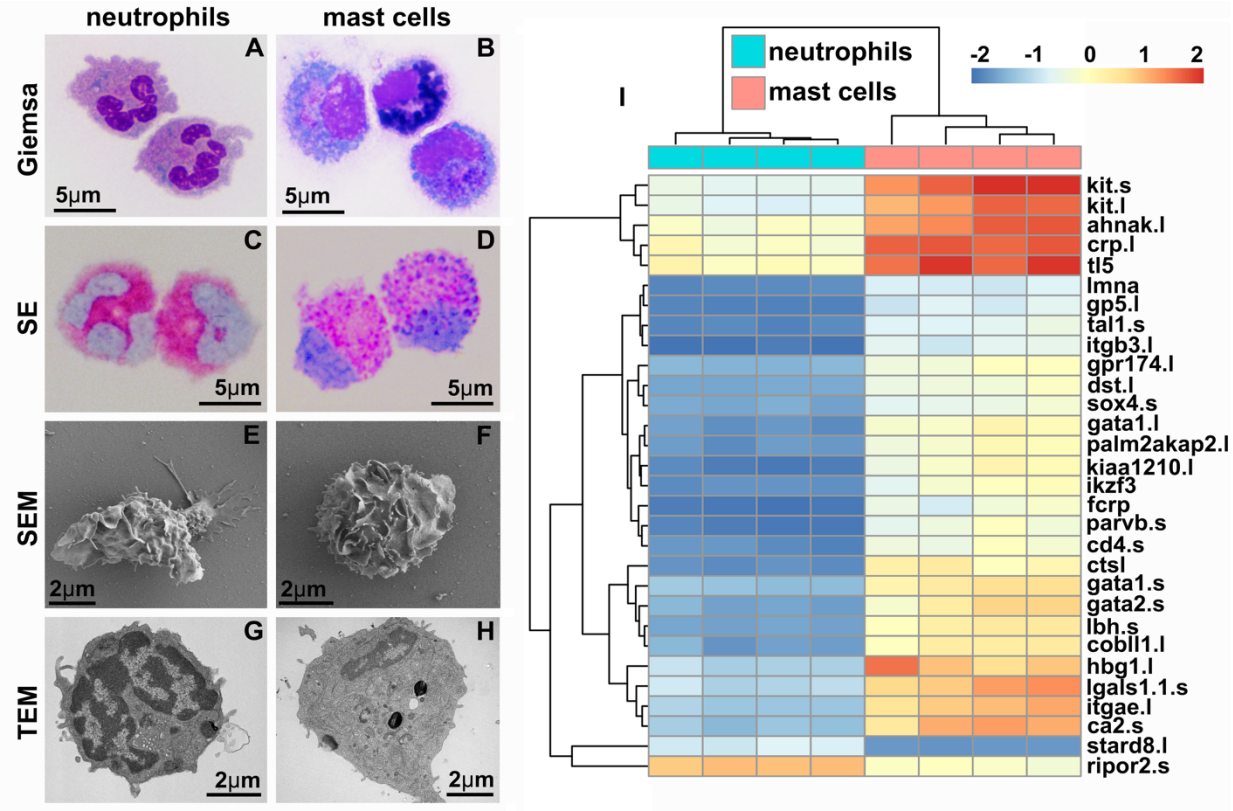

Figure 1. *X. laevis* bone marrow-derived mast cells possess classical mast cell cytology and transcriptional profiles. Neutrophils (**A**, **C**, **E**, **G**) and mast cells (**B**, **D**, **F**, **H**) were stained with Giemsa (**A**, **B**) and Leder to visualize specific esterase activity (SE) (**C**, **D**) or imaged with scanning and transmission electron microscopy (SEM: **E**, **F** and TEM: **G**, **H**). (**I**) Heat map of the top 30 differentially expressed genes (DEGs) identified with RNA sequencing analyses of *X. laevis* mast cell (*N*=4) and neutrophil (*N*=4) cultures. Log_2fold change in expression represented as color scale.

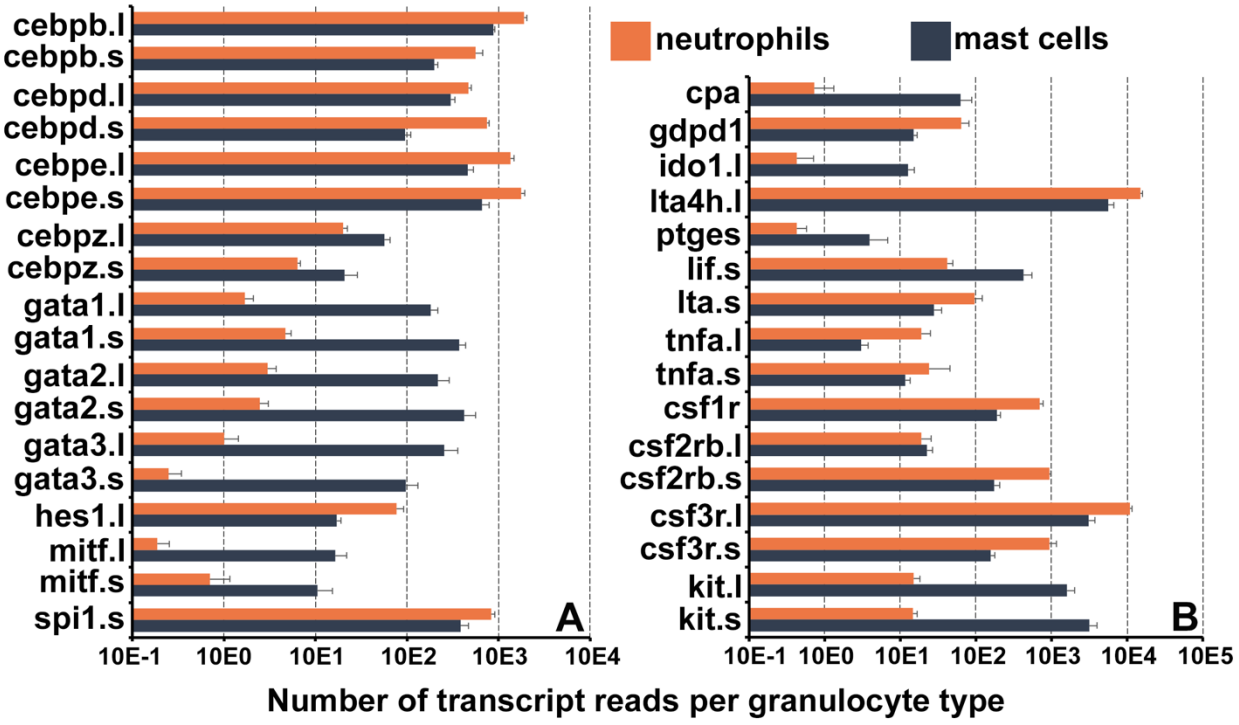

Figure 2. Frog mast cells and neutrophils possess gene profiles similar to their mammalian counterparts. The differentially expressed genes from the RNA sequencing analyses of *X. laevis* mast cells and neutrophil cultures were profiled for those encoding (**A**) transcription factors associated with mast cell- or neutrophil-specific lineages and (**B**) granulocyte antimicrobial components and growth factor receptor genes. *All depicted genes were significantly differentially expressed between the two populations, N*=4 per group.

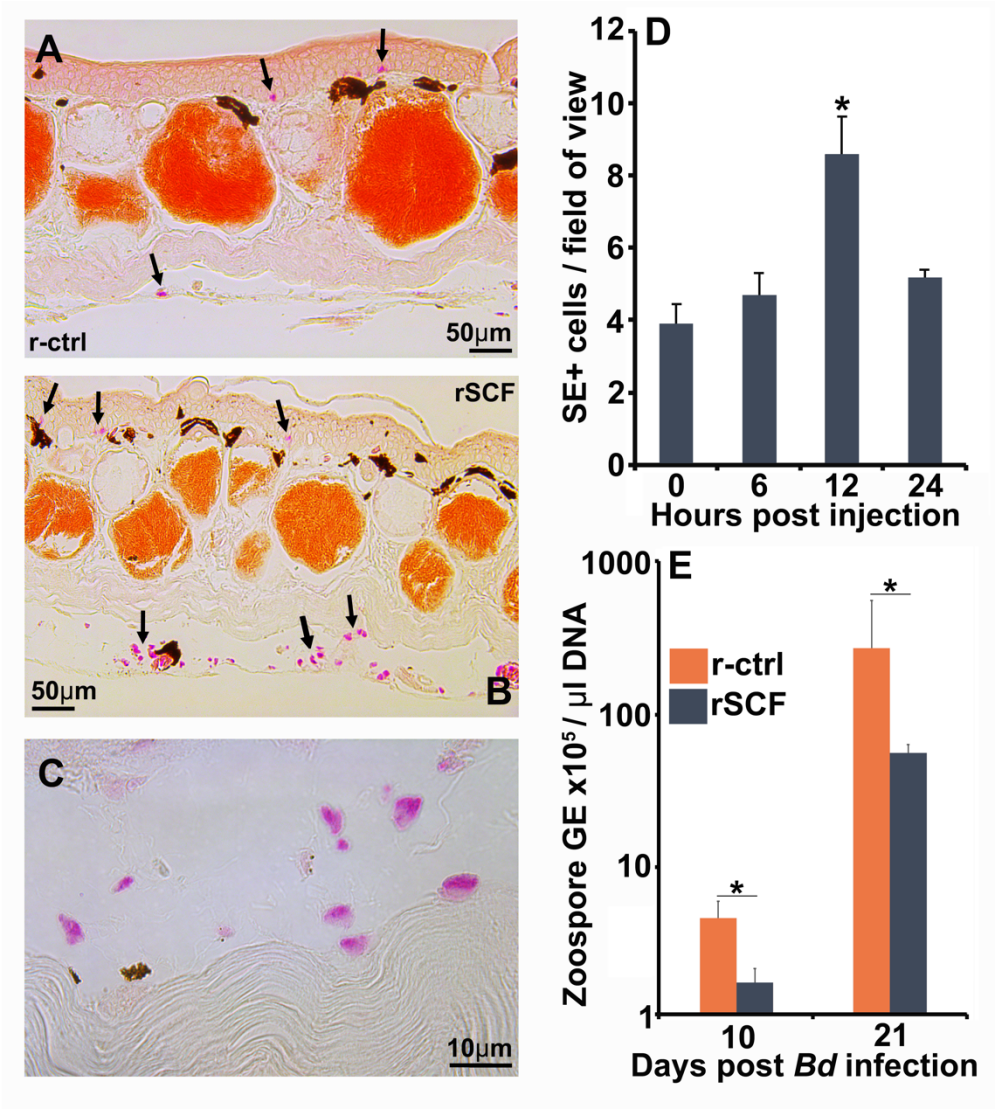

Figure. 3. Enriching frog cutaneous mast cells lowers *Bd* loads. Representative images of SE stained (**A**) control and (**B**) mast cell-enriched skin 12 hpi. (**C**) We confirmed the enriched population was composed of mono-morphonuclear cells. (**D**) Mast cell enrichment was optimized across several time points by quantifying SE-positive cells per field of view under 40x magnification. Results represent means ± SEM from 3 animals per time point (2 experimental repeats). (**E**) Mast cell-enriched and control dorsal skins were collected from *X. laevis* 10- and 21-dpi. *Bd* loads are represented as the number of zoospore genomic equivalents (GE) x 10^5 per µl of total input DNA. Time points were analyzed independently. Results represent means ± SEM from 7 animals per experimental group (N=7). Asterisks indicate significance: $p < 0.05$ by (**D**) one-way ANOVA with Tukey post-hoc analysis or (**E**) Student's t-test.

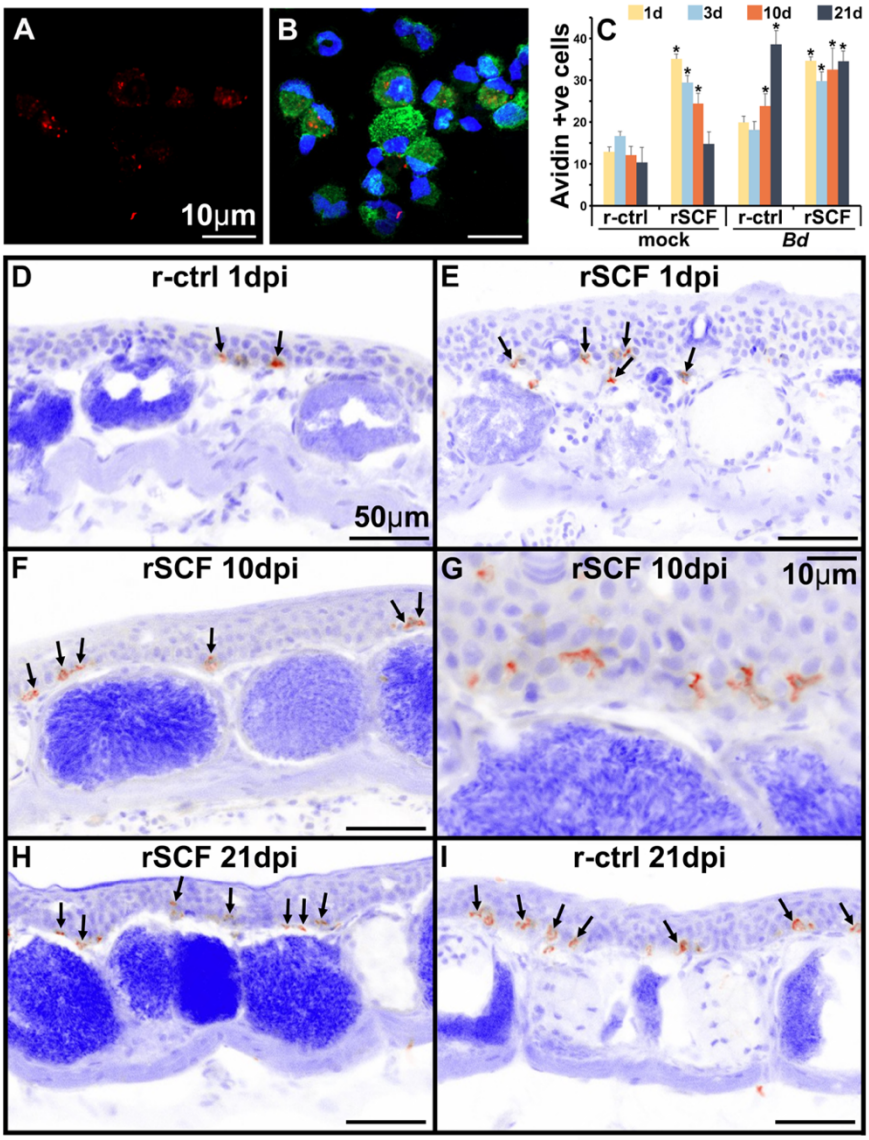

Figure. 4. Heparin content and skin localization of frog mast cells. Frogs were administered r-ctrl or rSCF subcutaneously, mock or *Bd*-challenged and skin examined after 1, 3, 10 and 21 dpi. (**A, B**) Representative images (cultures derived from 5 individual frogs) of bone marrow-derived frog mast cells, stained with fluorescently labeled avidin to visualize the heparin-containing mast cells (avidin: red; nuclei: blue; actin: green). (**C-I**) Skin tissue from control (r-ctrl) or mast cell-enriched (rSCF), mock- (not shown) and *Bd*-infected (**D-I**) *X. laevis* were stained with fluorescently labeled avidin to visualize mast cells therein (N=6 animals per treatment group). Images were inverted in ImageJ for greater contrast and visibility. (**C**) Heparin-containing mast cells were enumerated and depicted as means $\pm$ SEM of heparin-positive cells per field of view, N=6 animals per treatment group. Asterisks indicate statistical significance from r-ctrl: $p < 0.05$. Representative images of heparin-containing mast cells in the skins of (**D**) r-ctrl animals 1 dpi; (**E**) rSCF-administered frogs 1 dpi; (**F, G**) rSCF-administered frogs 10 dpi; (**H**) rSCF-administered frogs 21 dpi and (**I**) r-ctrl-treated animals 21 dpi with *Bd*.

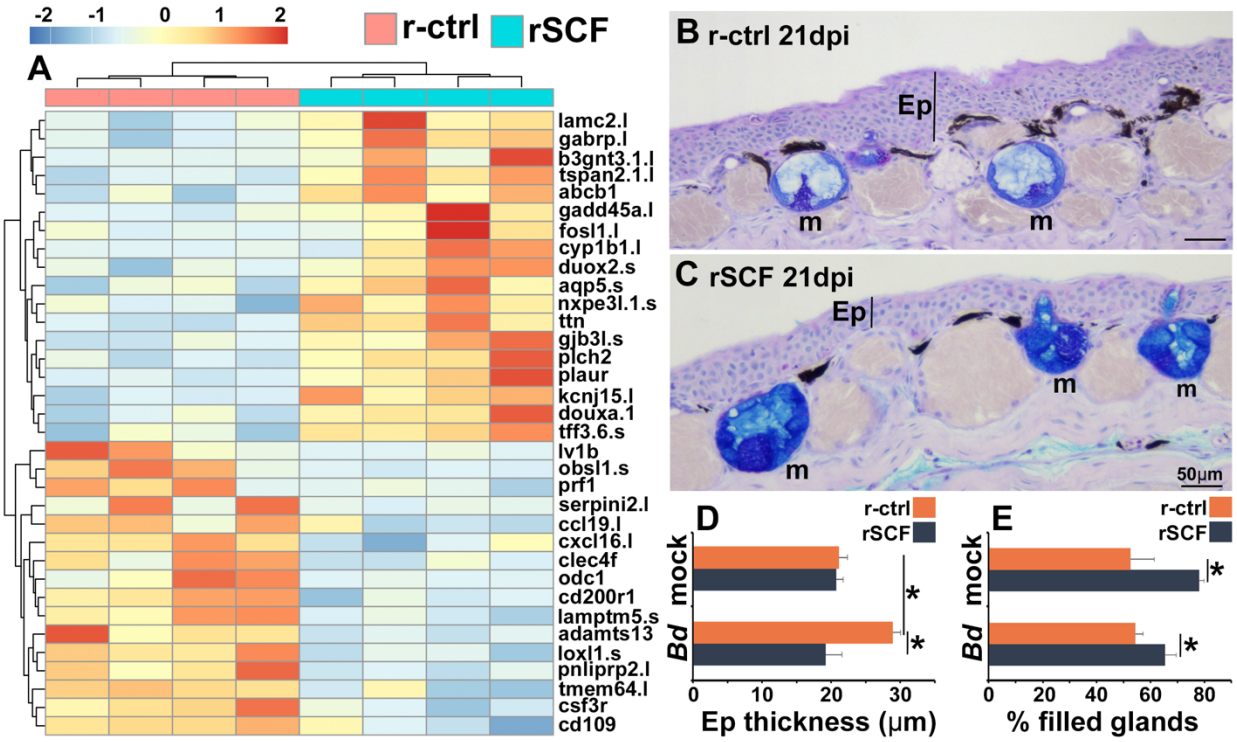

Figure. 5. Consequences of cutaneous mast cell enrichment. (**A**) RNAseq analysis of skin tissue from control (r-ctrl) or mast cell-enriched (rSCF) *Bd*-infected *X. laevis* at 21 dpi. Heat map of the top 30 DEGs, numbers matched to colors represent $\log^2$ fold change in expression, $N = 4$ r-ctrl-treated, *Bd*-infected and 4 rSCF-treated, *Bd*-infected skin samples. (**B** & **C**) Representative images of control and mast cell-enriched, *Bd*-infected skins, 21 dpi, demonstrating differences in epidermal thickening and mucus gland filling. Mucin content was visualized in cutaneous mucus glands with Alcian Blue/PAS stain. Mucus glands are denoted by 'm', and epithelia are denoted by 'Ep'. ImageJ software was used to determine the means $\pm$ SEM of (**D**) skin epithelial thickness and (**E**) percent mucus gland filling (N=6). Asterisks indicate significance: $p < 0.05$ by one-way ANOVA with Tukey post-hoc analysis.

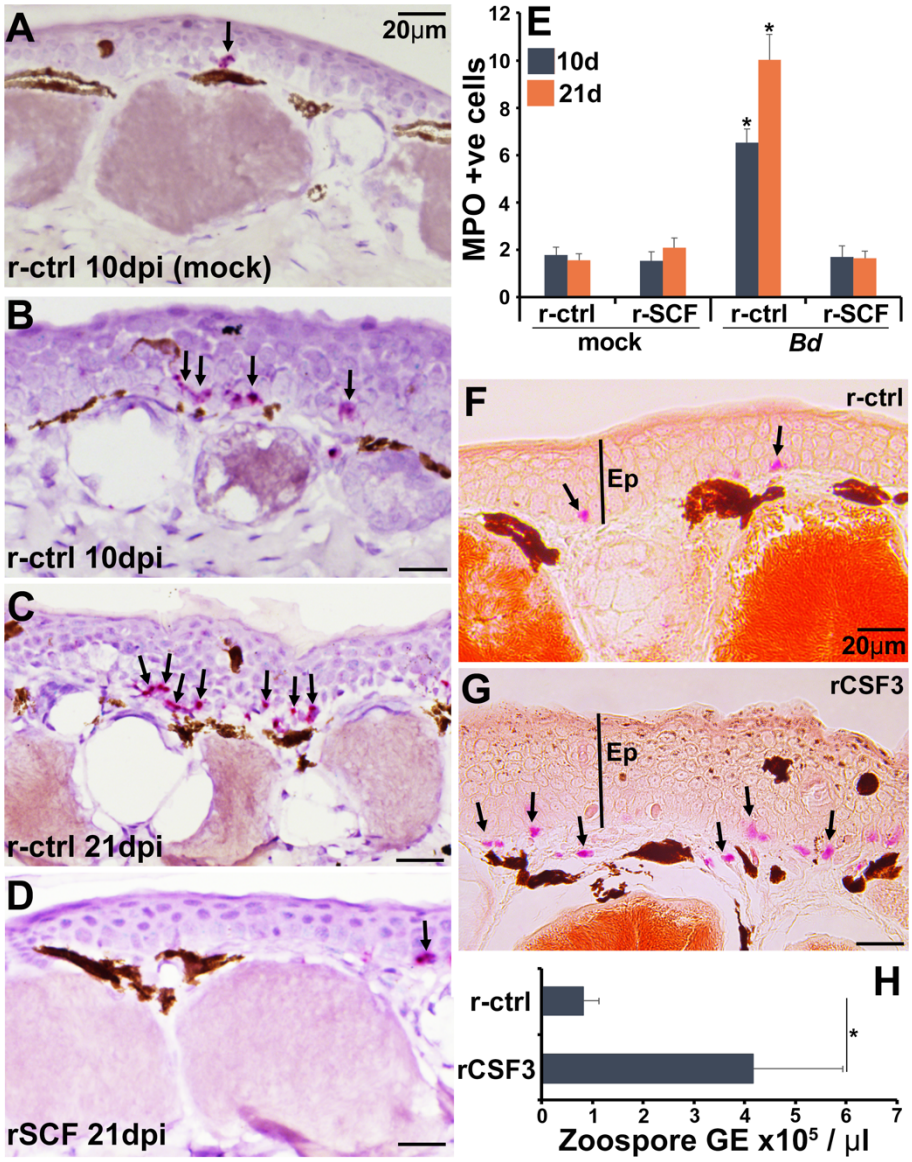

Figure 6. Consequences of cutaneous neutrophil enrichment. (**A-E**) Frogs were administered with r-ctrl or rSCF, mock- or *Bd*-infected and examined *in situ* for neutrophil content via by RNAScope analyses of myeloperoxidase (mpo) transcripts. Representative images of (**A**) r-ctrl-injected frog skins 10 days post mock infection; (**B**) r-ctrl-injected frog skins 10 days post *Bd* infection; (**C**) r-ctrl-injected frog skins 21 days post *Bd* infection; and (**D**) r-SCF-administered frog skins 21 days post *Bd* infection. (**E**) Means ± SEM of mpo-positive neutrophils per field of view of r-ctrl- and rSCF-administered, mock- or *Bd*-challenged frog skins 10 or 21 dpi, (N=6). Asterisks indicate significance from control: $p < 0.05$ by one-way ANOVA with Tukey post-hoc analysis. Representative specific-esterase staining of skin tissues from frogs were administered with (**F**) r-ctrl or (**G**) rCSF3, N=4. Arrows denote specific esterase-positive cells. Ep: epithelium. (**H**) *Bd* loads in control and neutrophil-enriched skin tissues 7 dpi, N=6. Asterisks indicate significance: $p < 0.05$ by one-way ANOVA with Tukey post-hoc analysis.

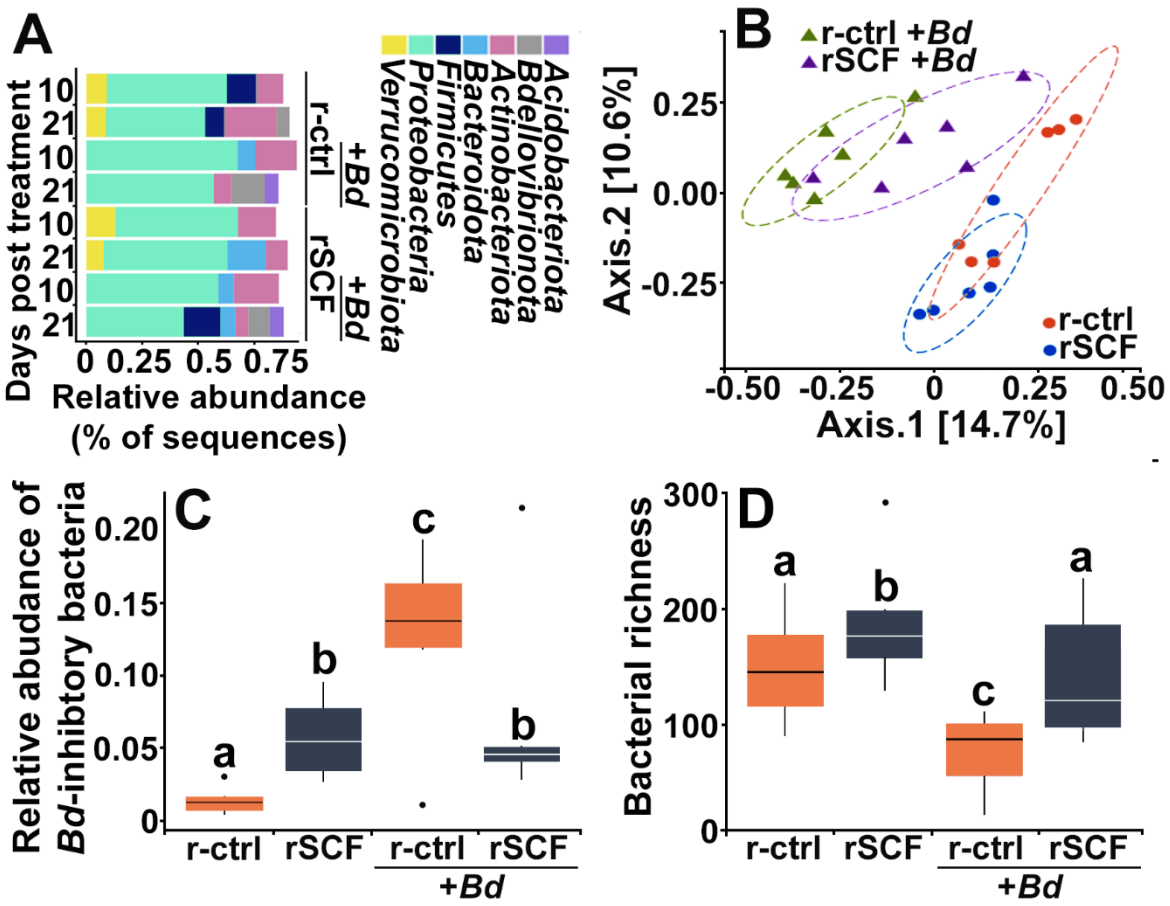

Figure 7. Cutaneous mast cells protect skin microbial communities. Control (r-ctrl-injected) or mast cell-enriched (rSCF-injected) *X. laevis* were mock-infected or challenged with *Bd* for 21 days. (**A**) Microbial phyla distribution across groups. Low abundance phyla (< 5% relative abundance are not shown). At 10 dpi (**B**) community composition (Jaccard distances shown with 80% confidence ellipses) differed among all treatments. (**C**) Relative abundance of *Bd*-inhibitory bacteria and (**D**) bacterial richness were examined in control and mast cell enriched frogs, 10 days post *Bd* or mock challenge. Letters above bars indicate statistically different groups.

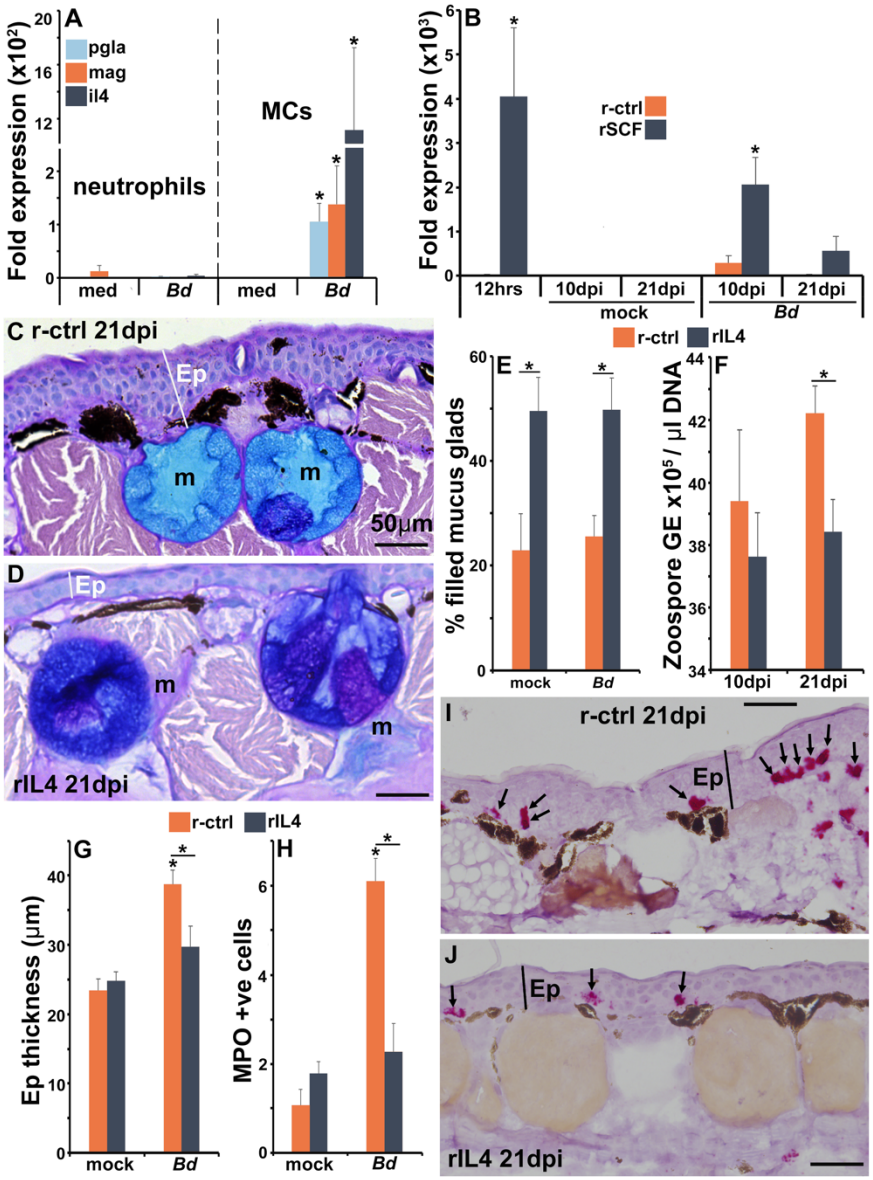

Figure 8. The roles of IL4 in mast cell-mediated skin anti-*Bd* protection. (**A**) Mast cells and neutrophils derived from bone marrow of 6 individual frogs (*N*=6) were co-cultured with *Bd* (5 fungal cells per granulocyte) for 6 hrs prior to gene expression analyses of the antimicrobial peptide genes PGLa (*pgla*) and magainin (*mag*) or interleukin-4 (*il4*). (**B**) *Il4* gene expression in skins of control and mast cell-enriched, mock- or *Bd*-infected animals, *N*=6. Representative images of frogs administered with (**C**) r-ctrl or (**D**) rIL4 and infected with *Bd* for 21 days, *N*=7. Ep: epidermis; m: mucus gland. Means ± SEM of (**E**) percent mucus gland filling, (**F**) skin *Bd* loads, (**G**) epidermal thickness and (**H**) mpo-positive neutrophils, per field of view of r-ctrl- and rSCF-administered, mock- or *Bd*-challenged frog skins 21 dpi, (*N*=7). Representative images of mpo-positive neutrophils in (**I**) control and (**J**) rIL4-treated frog skins, 21 dpi. Ep: epidermis; arrows: mpo-positive neutrophils. Asterisks indicate significance: $p < 0.05$ by one-way ANOVA with Tukey post-hoc analysis.

SUPPLEMENTARY MATERIALS

Production of recombinant cytokines: The *X. laevis* SCF and CSF3 sequences representing the signal peptide-cleaved transcripts were ligated into the pMIB/V5 His A insect expression vectors (Invitrogen). SCF-ligated, CSF3-ligated, or empty vectors were transfected into Sf9 insect cells (cellfectin II, Invitrogen). Recombinant proteins contain a V5 epitope, and western blot with an anti-V5-HRP antibody (Sigma) confirmed their presence. Positive transfectants were selected using 10 µg/mL blasticidin (Gibco). Expression cultures were scaled up to 500 mL liquid cultures, grown for 5 days, pelleted by centrifugation, and the supernatants collected. Supernatants were dialyzed overnight at 4°C against 150 mM sodium phosphate, concentrated against polyethylene glycol flakes (8 kDa) at 4°C, dialyzed overnight at 4°C against 150 mM sodium phosphate, and passed through Ni-NTA agarose columns (Qiagen). Columns were washed with 2 × 10 volumes of high stringency wash buffer (0.5% Tween 20, 50 mM Sodium Phosphate, 500 mM Sodium Chloride, 100 mM Imidazole) and 5 x 10 volumes of low stringency wash buffer (as above but with 40 mM Imidazole). Recombinant proteins were eluted with 250 mM imidazole. After recombinant protein purification, a halt protease inhibitor cocktail (containing AEBSF, aprotinin, bestatin, E-64, leupeptin and pepstatin A; Thermo Scientific) was added. Intact recombinant protein presence was confirmed again by western blot and the protein concentrations quantified by Bradford protein assays (BioRad). Protein aliquots were stored at -20°C until use.

Bone marrow granulocyte cultures: Bone marrow cells were isolated as previously described [68]. Briefly, adult *X. laevis* (approximately one year old) were euthanized in 5% tricaine mesylate followed by cervical dislocation. Femurs were removed and washed in ice-cold Amphibian-PBS (A-PBS) in sterile conditions. Each femur was flushed with 5 mL of A-PBS. Red blood cells were removed from culture via a differential gradient generated with 51% Percoll. Bone marrow cell counts were generated using trypan blue exclusion and cells were seeded at a density of 10^4 cells/well for gene expression experiments, $5x10^4$ cells/well for histology analyses, and 10^5 cells/well for electron microscopy analyses.

Histology: Paraffin-embedded tissue sections (5 µm) were deparaffinized, rehydrated through A-PBS, and stained with Naphthol AS-D Chloroacetate (specific esterase; Sigma) or Alcian Blue/PAS (Newcomer, Middleton, WI) according to the manufacturers' instructions and optimized

for *Xenopus* skin tissues. Cells collected from *in vitro* cultures were cytocentrifuged onto glass microscope slides (VWR). Cells were stained immediately with Giemsa (Sigma) for 7 minutes or fixed with 10% neutral buffered formalin for 30 minutes and stained with specific esterase according to the manufacturers' instructions. Slides stained with Alcian Blue/PAS (Newcomer) were used to quantify mucin content from *in vivo* experiments. Images were taken using identical microscope settings under 20x magnification. Images were converted to 8-bit in Fiji by ImageJ and threshold adjusted such that positive staining for mucus was captured within the mucus glands (threshold held constant across images). The percentage of each mucus gland positively stained and the average percent-positive per field of view were subsequently calculated. Positive staining of both acidic and neutral mucins was included in analyses. ImageJ was also used for epidermal thickness analyses, using scale bars in the images to calibrate and measure epidermal thickness. All slides were imaged with a Leica DMi8 Inverted Fluorescent Microscope with all mucus glands assessed for each respective frog skin section (Leica Microsystems, Davie, FL).

An RNAScope ISH Kit (ACD Bio) and a *X. laevis* myeloperoxidase (mpo)-specific probe (ACD Bio) were used according to manufacturer's instructions to visualize mpo-positive neutrophils in frog skin tissues.

Towards avidin staining, skin tissues were fixed in 4% paraformaldehyde, washed with saline, cryo-protected in 15% then 30% sucrose, flash-frozen in optimal cutting temperature (OCT) compound (Fisher) and cryo-sectioned onto microscope slides (Fisher). Frozen sections were stained with Texas red-conjugated avidin (ThermoFisher) and DAPI (ThermoFisher) and glass cover slips mounted with Prolong Antifade mounting media (ThermoFisher). Tissues were imaged using a Zeiss LSCM-800 confocal microscope. For each slide, 15 fields of view were enumerated at ×20 (Plan-Apochromat 20×/0.75) objective. Images were inversed in ImageJ to improve contrast and resolution of heparin-positive skin mast cells.

Analyses of immune gene expression and *Bd* skin loads: Cells and tissues were homogenized in Trizol reagent, flash frozen on dry ice, and stored at -80°C until RNA and DNA isolation. RNA isolation was performed using Trizol according to the manufacturer's directions. RNA-Seq is described in detail below. For qRT-PCR gene expression analysis, RNA (500 ng/sample) was reverse transcribed into cDNA using cDNA qscript supermix (Quantabio, Beverly, MA). Following RNA extraction, back extraction buffer (4 M guanidinethiocyanate, 50 mM sodium

citrate, 1 M Tris pH 8.0) was mixed with the remaining Trizol layer and centrifuged to isolate the DNA-containing aqueous phase. DNA was precipitated overnight with isopropanol, pelleted by centrifugation, washed with 80% ethanol, and resuspended in TE buffer (10 mM Tris pH 8.0, 1 mM EDTA). DNA was purified by phenol:chloroform extraction and resuspended in molecular grade water (VWR).

Quantitative gene expression analyses for both *Bd* and *X. laevis* cells and tissues were performed using the CFX96 Real-Time System (Bio-Rad Laboratories, Hercules, CA) and iTaq Universal SYBR Green Supermix (Bio-Rad Laboratories). The Bio-Rad CFX Manager software (SDS) was employed for all expression analysis. All expression analyses were conducted using the ΔΔCt method relative to the *gapdh* endogenous control gene for *X. laevis.* Fungal load quantification was assessed by absolute qPCR. Isolated *Bd* DNA (JEL 197 isolate) was serially diluted and used as the standard curve. Primers were designed and validated against the *Bd* ribosomal RNA internal transcribed spacer 1 (ITS1). The primers used are listed in Table S1.

Analyses of mucus *Bd*-killing capacities: Mucosomes were collected from mast cell- or vector-enriched *X. laevis* that were either mock- or *Bd*-infected for 10 or 21 days. To this end, individual *X. laevis* were soaked in a 5 mL water bath for 1 hour. Each water sample was then lyophilized, reconstituted with 500 µl of molecular grade water, and passed through a sterile cell strainer to remove large debris.

Bd was seeded in opaque white 96-well plates (20,000 zoospores in 50 µl of tryptone broth / well). Next, 50 µl of mucosome solution was added to each well (100 µl total well volume) in three replicate wells per individual *X. laevis* mucosome. Mucosomes, tryptone broth, and water were each plated alone as controls. Plates were sealed with parafilm and incubated at 19°C for 16 hrs with gentle mixing (20 rpm).

Zoospore viability was determined with the CellTiter-Glo 2.0 Cell Viability assay kit (Promega) according to the manufacturer's instructions and using a SpectraMax plate reader (Molecular Devices, San Jose, CA). Luminescence readings were fitted to a standard curve (descending proportions of heat-killed zoospores to viable zoospores) to calculate the number of viable zoospores in each well. Zoospores were heated-killed at 65°C for 15 mins.

Skin microbiome analyses: All analyses were performed in the R environment version 4.0.3 (R Core Team, 2020). Demultiplexed reads were imported from Basespace into R environment for sequence processing. Package "dada2"[71] was used to perform quality filtering using their standard filtering parameters (*i.e.*, maxEE = 2), which collapsed high quality reads into amplicon sequence variant (ASV) and removed chimeras. Bacterial taxonomy was assigned using Silva version 138.1. The R package "phyloseq"[72] was used to import and merge the final ASV table, taxonomy table, and metadata to create a phyloseq object to perform further analyses. Sequences classified as cyanobacteria/chloroplast and those unclassified at kingdom were removed. Singletons were filtered out (*i.e.*, ASVs with only one sequence read in one individual). The R package "decontam"[73] was used to remove potential contaminants using the method "combined." The ZymoBIOMICS microbial community standards (positive controls) were analyzed, and we found genera in similar relative abundances as described by Zymo.

To determine how *Bd* and mast cell treatments impacted skin microbiomes, the microbiome structure was examined. The components of microbiome structure were: ASV richness (measured as *Bd*-inhibitory ASV richness and total ASV richness), microbial composition (measured by Jaccard and Bray-Curtis distances), and sequence abundance of *Bd*-inhibitory ASVs (measured as individual *Bd*-inhibitory ASV sequence counts and total relative abundance of *Bd*-inhibitory ASVs). To characterize variation in microbiome structure, Mast Cell (mast cell normal and mast cell+), *Bd* (*Bd*- and *Bd*+) and their interaction as explanatory variables at two-time points Day 10 and Day 21 post *Bd* infection were included. For this characterization, log-transformed ASV richness in ANOVAs, microbial composition measures in PERMANOVAs and log-transformed raw sequence counts in ANOVAs (with post-hoc corrections for multiple comparisons) were used. For identification of *Bd*-inhibitory ASVs, methods as described in by Jimenez *et al*., 2022[74] were followed.

Days 10 and 21 post *Bd* infection were chose for these analyses, since they represent an intermediate and a later timepoint of infection.

Table S1. List of primer sequences

Target Name	Primer Sequence (5'→ 3')
***Bd* its1 sense**	GCCATATGTCACGAGTCGAA
***Bd* its1 antisense**	GCCAAGAGATCCGTTGTCA
gapdh sense	GACACTCACTCCTCCATCTTTG
gapdh antisense	TGCTGTAGCCGCATTCATTA
hdc sense	GAATCTGAAAGCTGGGAGAGAA
hdc antisense	GATGTCAGGGCAGGAAAGTAG
il4 sense	GACATCAAGGACACCTGAAGAA
il4 antisense	GTCACAGGGAATCGGTACTAAAC
mag sense	GGCCTTTGCAGATGAAGATTTAG
mag antisense	CTACTGCTTCTGCATCTCGTT
pgla sense	CTGCACTCTGTGCAACCATAA
pgla antisense	CTCCAGCTTTAGATGCCATTCC

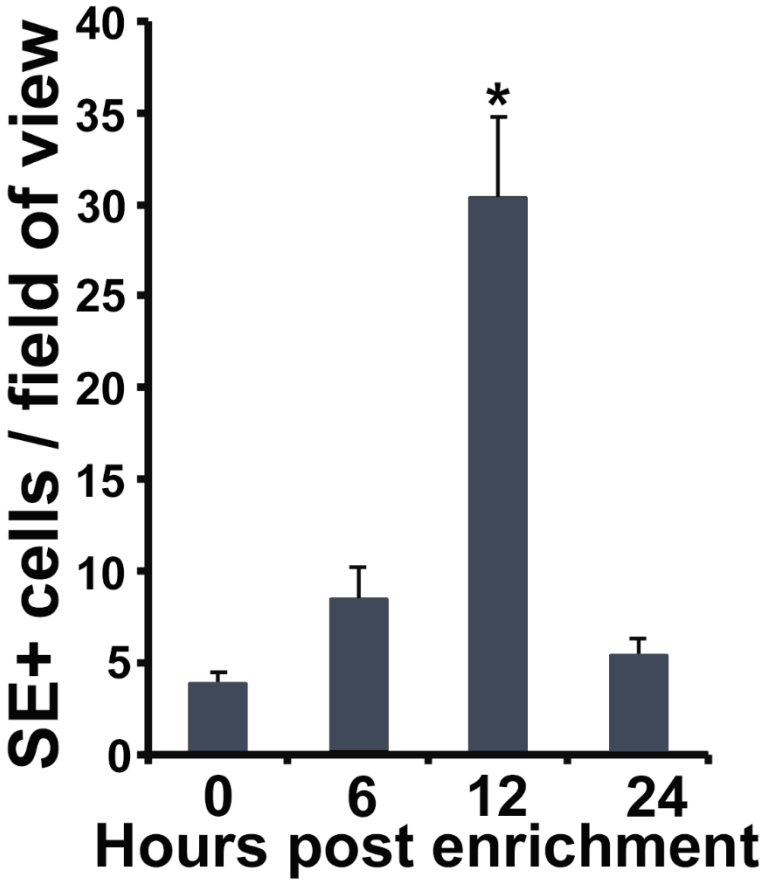

Figure S1. Enrichment of neutrophils in frog skins. Frogs were administered with rCSF3 subcutaneously and their skins examined for specific esterase activity at 0, 6, 12 and 24 hrs post injection. Results are means + SEM of SE-positive cells per field of view from 4 animals per time point (*N*=4). Asterisks indicate significance: $p < 0.05$ by one-way ANOVA with Tukey post-hoc analysis.

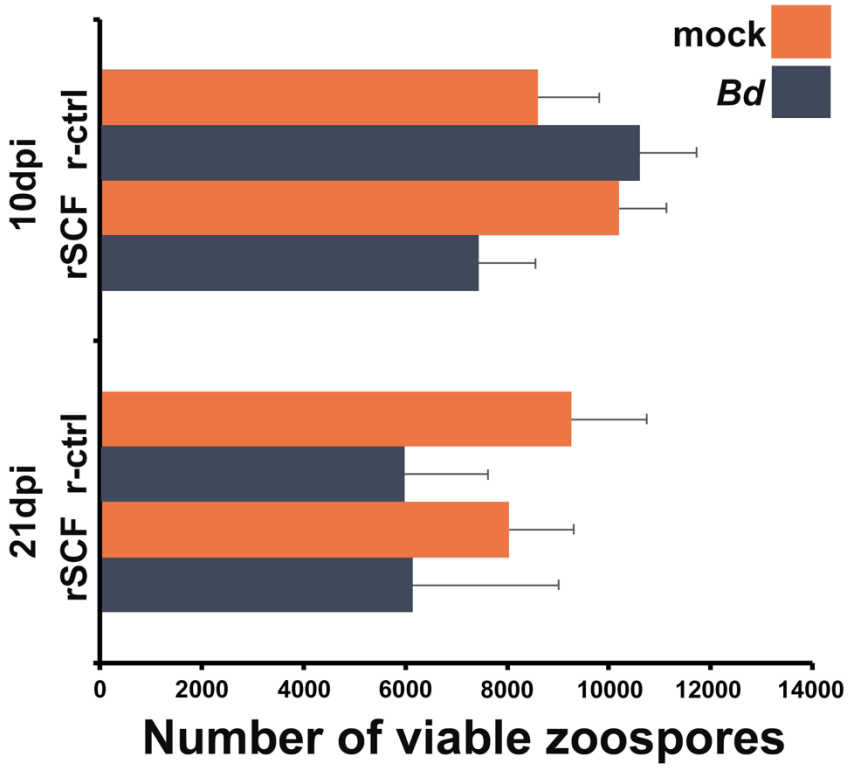

Figure S2. Mucosomes from mast cell-enriched frogs do not confer *Bd* killing. Differences in musocome-killing capacities were determined by incubating zoospores with total mucosome contents for 16 hrs. Mucosomes were acquired from 10- or 21-day mock- or *Bd*-infected *X. laevis* that were injected with rSCF (mast cell-enriched) or r-ctrl (control). Results are mean ± SEM and were analyzed via a two-way ANOVA; 10- and 21-day experimental groups were analyzed independently; alpha set at 0.05. N = 5 experimental animals per treatment group for 10 dpi analyses and N= 8 experimental animals per treatment group for 21 dpi analyses.

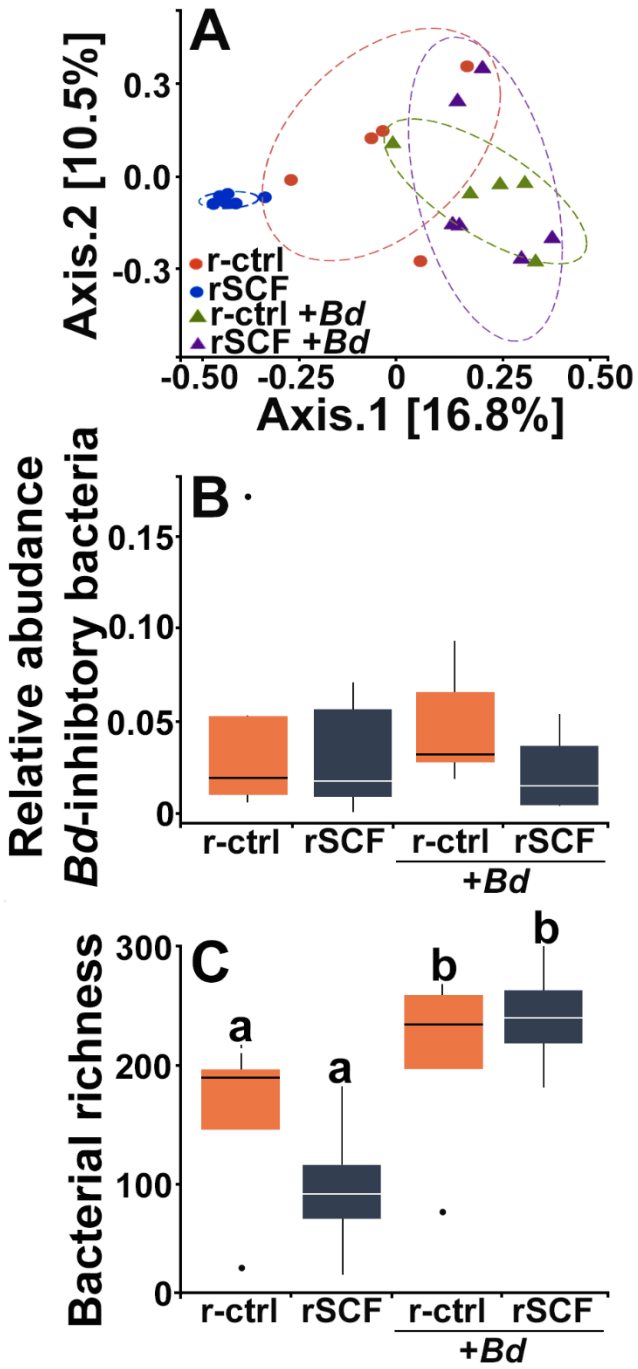

Figure S3. Mast cell enrichment protects frogs from *Bd*-mediated changes to skin microbiomes. At 21 days post mock or *Bd*-challenge, we examined (**A**) community composition (Jaccard distances shown with 80% confidence ellipses), (**F**) relative abundance of *Bd*-inhibitory bacteria and (**G**) bacterial richness. Letters above bars indicate statistically distinct groups.

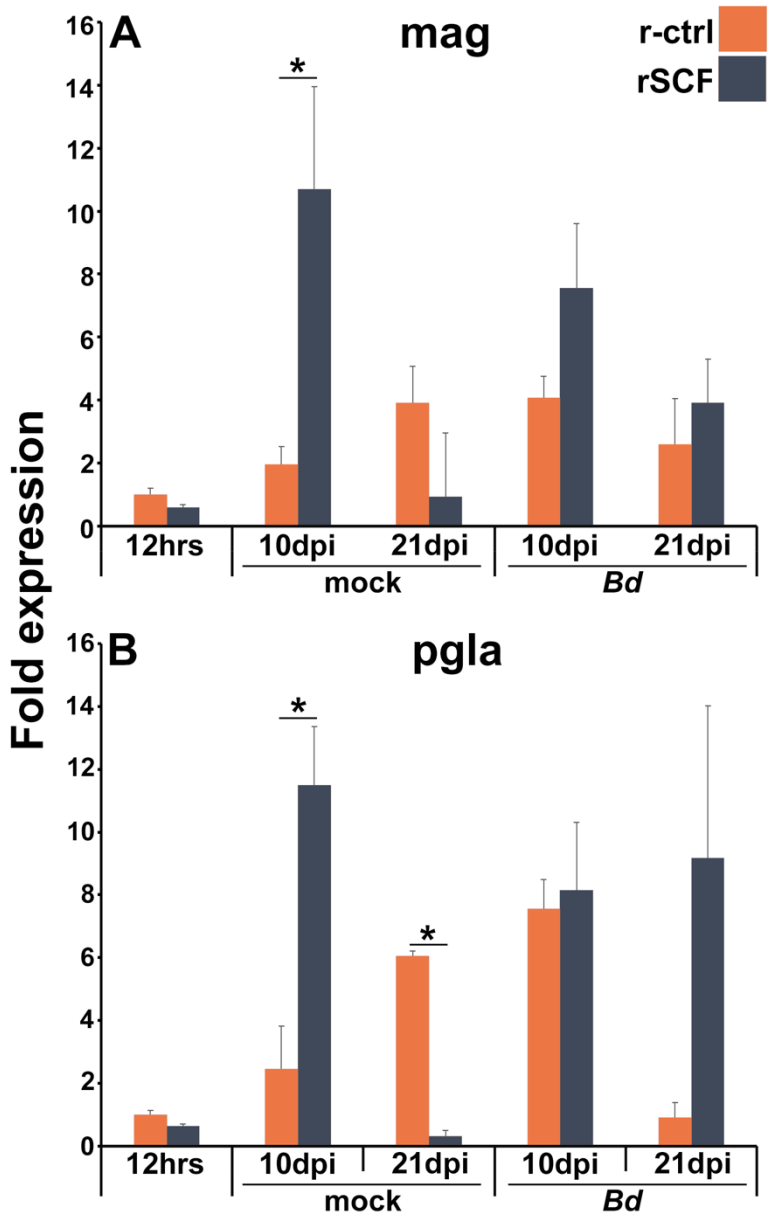

Figure S4. Expression of antimicrobial peptides in mast cell-enriched, Bd-infected frog skins. (**A**) *Magainin* (*mag*) and (**B**) *pgla* expression was examined in control and mast cell-enriched frog skins after 12 hrs of enrichment or after 10 or 21 days of mock- or *Bd*-challenge, *N*=6. Asterisks indicate significance: $p < 0.05$ by one-way ANOVA with Tukey post-hoc analysis.

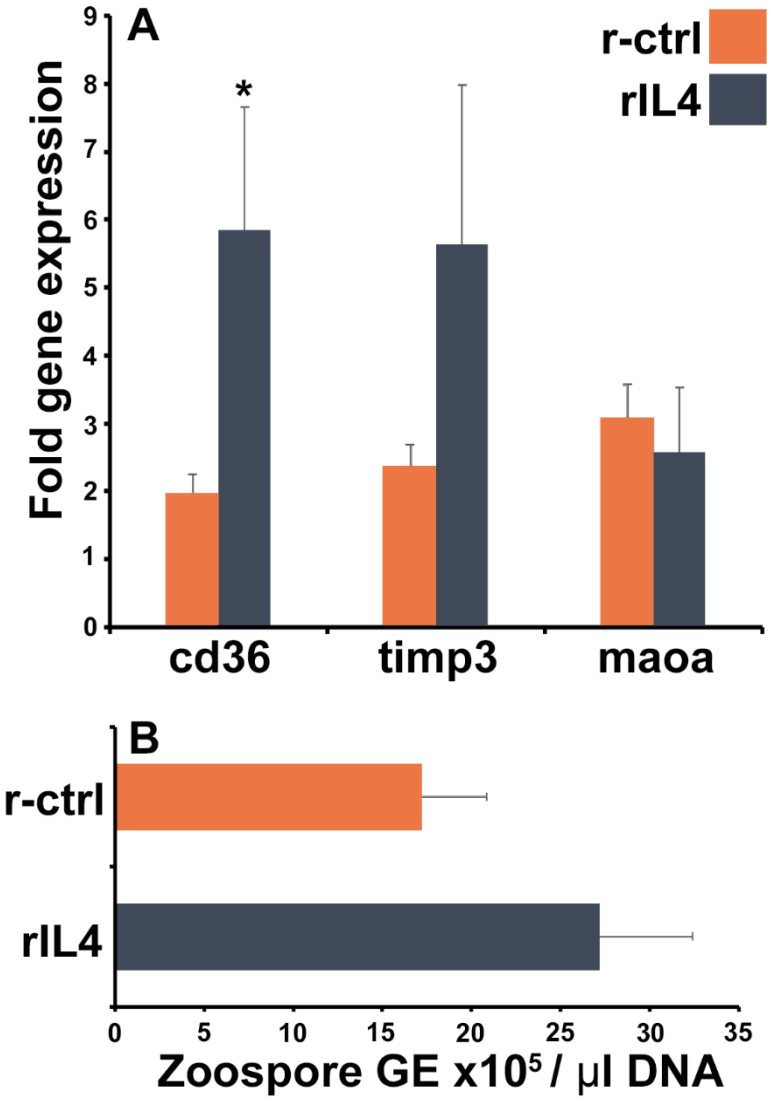

Figure S5. IL4 elicits hallmark gene expression but does not protect Bd-infected frogs. (**A**) Expression of selected genes in skin following subcutaneous injection of rIL4 (*N*=7). (**B**) Frogs were exposed to *Bd* and 24 hrs later injected subcutaneously with rIL4 or r-ctrl. Skin *Bd* loads were assessed 9 days following injection (*N*=8, per group). Asterisks denote statistical significance, $p < 0.05$ via ANOVA with Tukey post-hoc analysis.